Causes and consequences of the Messinian Salinity Crisis

Wout Krijgsman, Eelco J Rohling, Dan V Palcu, Fadl Raad, Udara Amarathunga, Rachel Flecker, Fabio Florindo, Andrew P Roberts, Francisco J Sierro, Giovanni Aloisi

Causes and consequences of the Messinian Salinity Crisis

Wout Krijgsman[1,†], Eelco J. Rohling[2], Dan V. Palcu[1], Fadl Raad[3], Udara Amarathunga[2], Rachel Flecker[4], Fabio Florindo[5], Andrew P. Roberts[2], Francisco J. Sierro[6], and Giovanni Aloisi[7]

[1] Department of Earth Sciences, Utrecht University, Utrecht, The Netherlands.
[2] Research School of Earth Sciences, Australian National University, Canberra, Australia.
[3] Department of Hydrogeology, University of Corsica Pasquale Paoli, Corte, France.
[4] BRIDGE, School of Geographical Sciences and Cabot Institute, University of Bristol, Bristol, UK.
[5] Istituto Nazionale di Geofisica e Vulcanologia, Rome, Italy.
[6] Department of Geology, University of Salamanca, Salamanca, Spain.
[7] Université Paris Cité, CNRS, Institut de Physique du Globe de Paris, Paris, France.
[†]e-mail: W.Krijgsman@uu.nl

Abstract

Salt giants are an intrinsic part of Earth's geological record and influence both regional and global climate and environments. In this Review, we summarize the causes and consequences of the Mediterranean Messinian salinity crisis (MSC; 5.97-5.33 million years ago), one of Earth's youngest and arguably best-studied salt giants. We emphasize that salt giant formation is more complex than development of a palaeo-hydrological imbalance. Instead, the tectonic setting of an evaporative basin largely determines the timing and mode of salt formation, with superimposed impacts of orbital-scale climate and sea-level fluctuations. Combined, these drivers triggered precipitation of carbonates, gypsum, halite, and even bittern salts in the Mediterranean, with well-defined orbital cyclicities in carbonate and gypsum phases. Salt extraction from the world ocean during evaporite and residual brine formation, rapid ion return during basin reconnection, and slow ion return due to evaporite weathering over geological timescales exert important feedbacks on global and regional environmental change over millennial to million year timescales. Our compilation of MSC boundary conditions highlights knowledge gaps for targeting future data collection campaigns and provides critical context to next-generation hydro-geochemical modelling of interactions between salt giants and environmental change.

Key points

1. Fifty years of Messinian salinity crisis research is summarized and general elements applicable to salt giant formation are highlighted.
2. Geodynamic and eustatic sea-level forcing are crucial for initiating and terminating salt giant formation with a subsidiary role for regional climate.
3. The main controls on evaporitic mineral precipitation are the freshwater deficit magnitude and the extent of water-exchange limitation between basin and ocean.
4. Evaluation of a new sea-level record for the 6.4 to 5.0 Ma time interval demonstrates that sea level is a viable driver of the prominent MSC sedimentary cyclicity in addition to orbital freshwater budget variation.
5. Formation and weathering of salt giants may be an important intermediate timescale carbon cycle driver.

Introduction

The opening and closure of oceans and seas by plate tectonic processes is often marked by formation of marginal basins that have restricted water-exchange with the open ocean. Under negative hydrological budgets, where freshwater loss by evaporation exceeds the supply from rivers and rainfall, periods of limited exchange with the open ocean can lead to precipitation of enormous evaporite deposits in the incipient or dying basin. Such "salt giants" formed episodically through Earth's history, including the Palaeozoic (Australia, USA, Russia, NW Europe), Mesozoic (South Atlantic, Gulf of Mexico), and Cenozoic (Mediterranean, Red Sea, Central Europe) eras[1,2]. Halite (NaCl) and gypsum/anhydrite ($CaSO_4$) extraction from seawater during salt giant formation can represent >5% of the total ocean dissolved salt content[3,4], which disrupts local ecosystems in evaporitic seas and modifies global ocean chemistry[5].

The Mediterranean Messinian salinity crisis (MSC) generated one of the youngest and arguably best-studied salt giants in Earth's history, even though most MSC deposits are buried below the Mediterranean seafloor and remain largely inaccessible to direct research[6]. Seismic profiles across deep basinal sequences and outcrops along tectonically uplifted marginal basins provide a picture of the spatial distribution of evaporite units (Fig. 1)[6–10]. The Late Miocene land-locked Mediterranean configuration amplified its responses to regional and global climate fluctuations, and caused distinct cycles in pre- and post-MSC deposits, facilitating construction of a detailed chronostratigraphic framework, tuned with precessional resolution (~20 kyr) to astronomical insolation curves[11–13]. This has resulted in a stratigraphic consensus scenario for the Mediterranean salt giant[6] that provides a foundation for high-resolution geochemical evaporite fingerprinting[14,15] and for observational and modelling studies of underlying forcing mechanisms[16,17].

Fifty years of MSC research demonstrates that salt giants do not form in basins that simply isolate and desiccate; rather, complex sub-basin settings play a crucial role in determining the timing and mode of salt formation[18,19] with contributions from various forcing mechanisms such as tectonics, sea-level change, and hydrological connectivity with the ocean[20]. In discussing the latest developments in MSC research here, we build from previous detailed overviews of MSC stratigraphy[6,21], Mediterranean evaporite distribution patterns[4,10], and

Atlantic-Mediterranean connectivity[20,22]. We also consider which elements are applicable more generally to salt giants, and reflect on their consequences for regional and global environmental change.

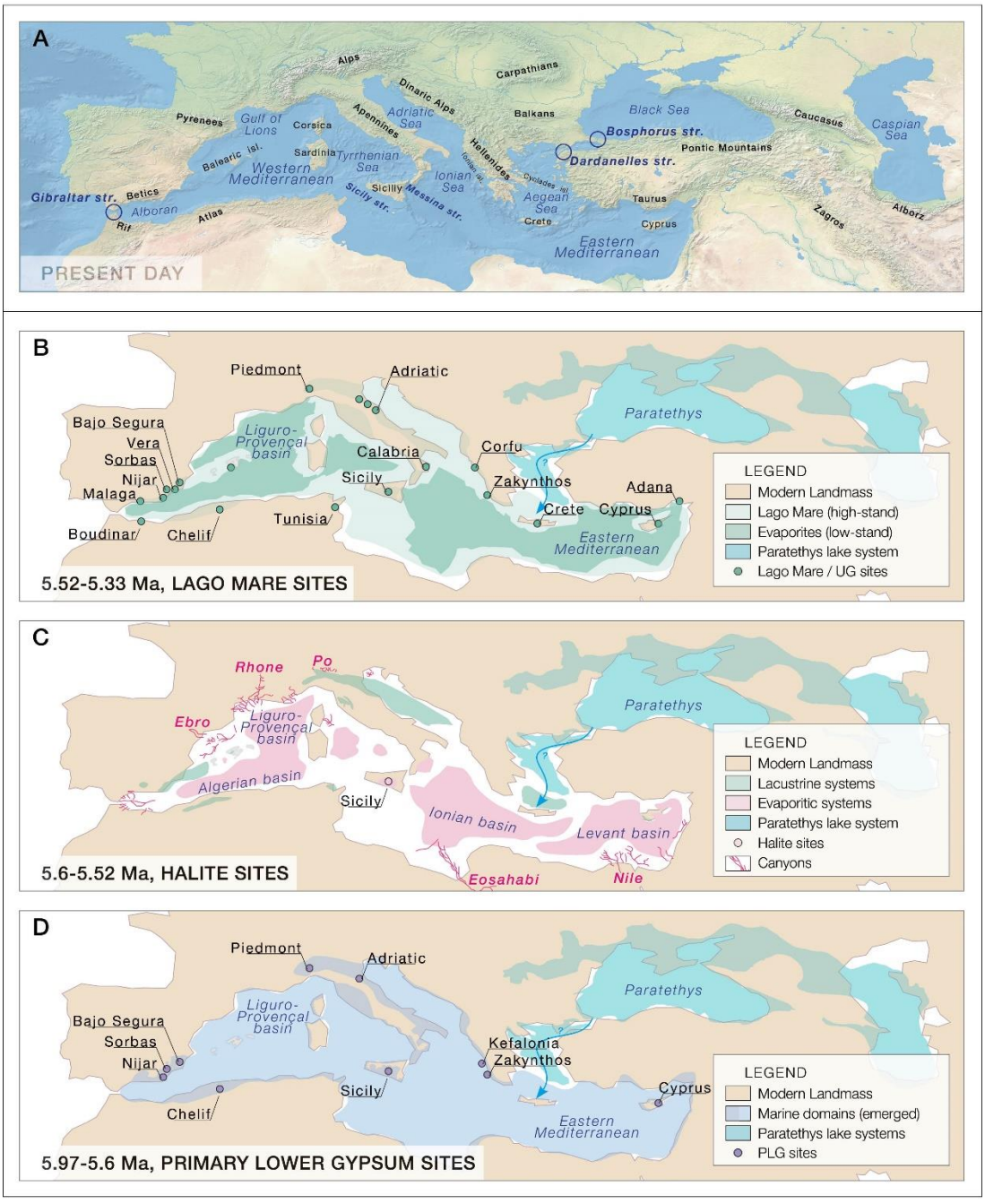

Figure 1. ***Mediterranean MSC evaporite stages. a*** *| Map of the Mediterranean region with the most important seas, straits, and mountain ranges labelled.* ***b-d*** *| Schematic maps of the Mediterranean and Paratethys seas during three evaporite stages[6] showing the main sites that crop out onshore.* ***b*** *| Non-marine upper gypsum (UG) stage with lacustrine deposits and Paratethyan fauna known as the "Lago Mare" in Mediterranean highstands and evaporites in lowstands;* ***c*** *| the desiccation stage during which halite was deposited; and* ***d*** *| water level during the marine primary lower gypsum (PLG) stage with Atlantic connectivity. For detailed distribution patterns from both offshore seismic and onshore field data, see recent literature[3,4,7–10,23–25].*

Evaporitic salt formation

Ocean chemistry has changed substantially over time[26]. One driver for this change is the precipitation and weathering of giant evaporite deposits. The most common marine evaporite minerals – carbonates, gypsum, anhydrite, halite, and the bittern salts (kainite, carnallite, bischofite) – precipitate from seawater when the concentration of their constituent ions (Na^+, Cl^-, Ca^{2+}, SO_4^{2-}, K^+, Mg^{2+}, HCO_3^-) exceeds a threshold known as the solubility product[27,28]. Ion concentration in evaporite basins depends both on water fluxes to, and the total water volume of, the marginal basin. Ions are added to these basins by water inflow from the ocean and rivers, and leave the basins only by outflow to the ocean or by mineral precipitation. The water volume in an evaporite basin is conserved if a sufficient oceanic connection exists, but it can decline through net evaporative draw-down if the connection becomes severely restricted or blocked; in both cases net evaporative freshwater removal raises the dissolved ion concentration in basin waters. The main controls on evaporitic mineral precipitation are, therefore, the magnitude of the freshwater deficit and the extent of water-exchange limitation between basin and ocean (Fig. 2a).

The simplest conceptual model for evaporitic salt formation considers a seawater volume disconnected from the ocean, subject to evaporative draw-down, while receiving no further ions from either seawater or river runoff. The Mediterranean salt giant, however, did not form under these conditions because complete evaporation of a 3,000 m-thick seawater column, with an average salinity of ~35 ‰, would leave behind only about 40 m of halite, a fraction of what is preserved in the deep central basins (~ 2.5 km of halite).

The evaporite-forming ion concentration in river water is, respectively, typically 1000 (Na^+, Cl^-), 100 (Mg^{2+}, SO_4^{2-}, K^+), and 10 (Ca^{2+}) times lower than in seawater[29,30]. Consequently, continental runoff influences marine evaporite mineral precipitation only if oceanic input is restricted severely or cut off entirely. A qualitative picture of the impact of ocean-continental water mixing on dissolved ions, as a function of seawater-exchange restriction, is shown in Fig. 2. Evaporites only evolve toward a “continental” mineralogical signature when the continental input dominates the oceanic source. This is the case for the Upper Gypsum succession on Sicily where non-oceanic Sr isotope data from both gypsum and ostracods suggests minimal Atlantic contribution[18]. The relative abundances of many other evaporite-forming ions are much higher in river water than in sea water

(in brackets): Mg^{2+}/Cl^- = 0.7 (0.1), SO_4^{2-}/Cl^- = 0.6 (0.052), Ca^{2+}/Cl^- = 1.2 (0.019), K^+/Cl^- = 0.05 (0.018), and HCO_3^-/Cl^- = 2.5 (0.004). Thus, when oceanic connection is highly restricted or blocked, carbonate and gypsum precipitation dominate the typical halite-dominated marine association[31].

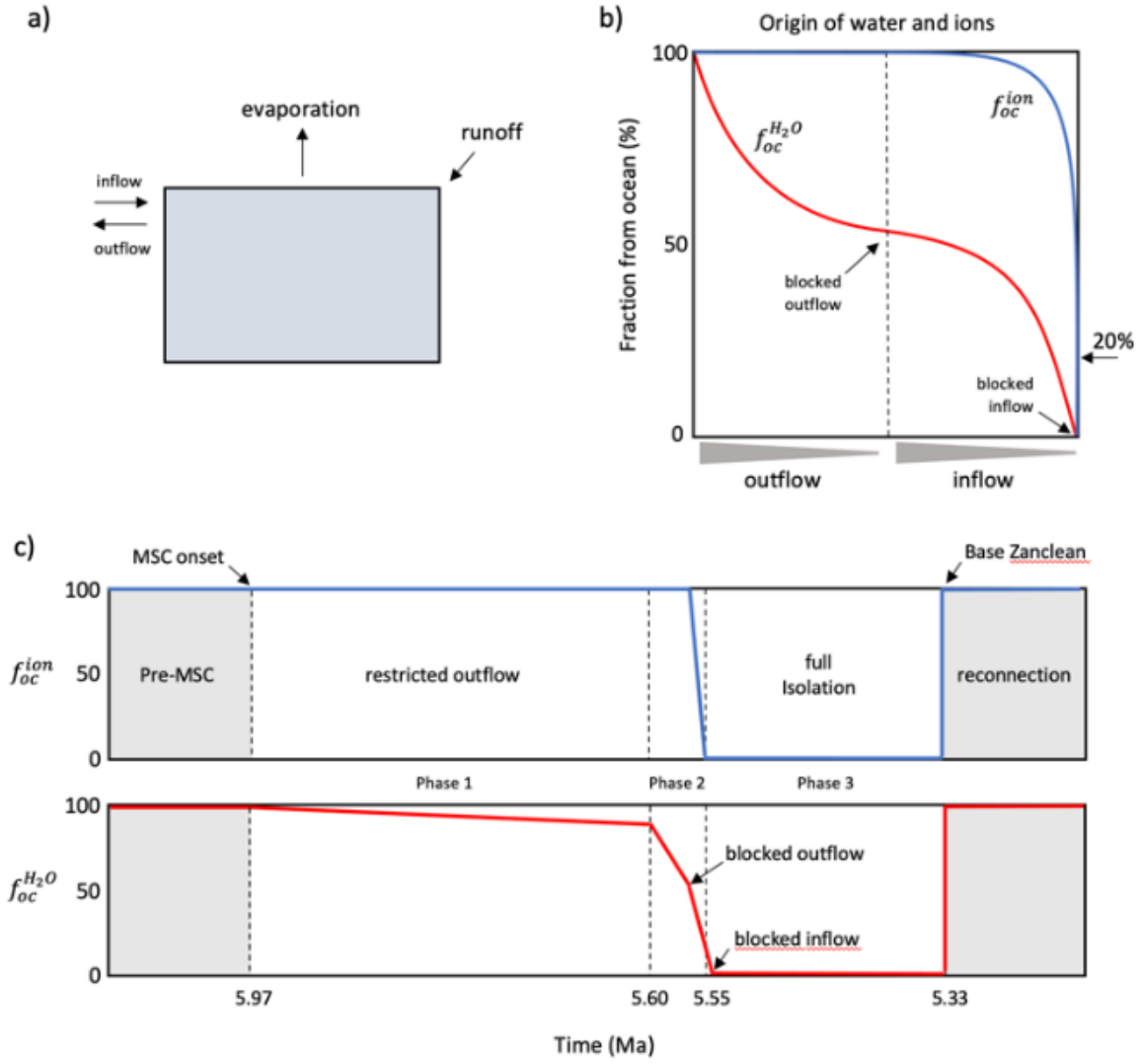

Figure 2. ***Evaporite geochemistry****.* ***a*** *| Controls on water and dissolved ion proportions from the ocean versus continental runoff during the MSC. Simplified water balance of an idealized marginal basin;* ***b*** *| fraction of water (red curve) and dissolved ions (blue curve) originating from the ocean as a function of seawater-exchange flux restriction at the sill separating the ocean from the marginal basin;* ***c*** *| idealized scheme for ocean water and ion fractions during the MSC; note that continental runoff becomes a relevant ion source to the basin only when its marine connection is restricted severely, or cut off completely, from the ocean*[36].

The Mediterranean salt giant

The first scientific reports of Mediterranean Messinian evaporites were by field geologists who documented ~100-m-thick gypsum units between marine sequences in several Italian basins[32,33]. In the 1970s, Deep Sea Drilling Project (DSDP) Leg 13 confirmed the widespread presence of evaporite units across the Mediterranean[3,34], although coring only reached the uppermost MSC successions. The presence of these evaporites led to the hypothesis that the Mediterranean became isolated from the Atlantic and desiccated almost entirely during the terminal Miocene[34,35]. The Mediterranean salt giant extracted an estimated 1.2 ± 0.1 km^3 (~7 to 10 %) of salts from the global ocean[4,34]. Detailed stratigraphic studies from onshore sequences and offshore seismic data indicate that the Mediterranean contains different evaporite successions (Fig. 1, 3)[6]. In addition to volumetrically minor K-Mg-salts (bittern salts) associated with halite, there are at least four main evaporitic deposit types observed in MSC successions now exposed on land: (1) evaporitic carbonates known as the Calcare di Base (Sicily)[36,37] and the Terminal Carbonate Complex (SE Spain)[38,39]; (2) predominantly marine gypsum known as the Primary Lower Gypsum unit (PLG: Spain, Italy)[15,40]; (3) halite (Sicily, Liguro-Provençal, Levant)[41]; and (4) gypsum with continental geochemical signatures in the so-called Upper Gypsum unit (UG: Sicily, Cyprus)[18,42]. Except for the halite in the western Mediterranean, all of these evaporites are interbedded with detrital clastics and/or hemipelagic sediments.

The depositional and stratigraphic architecture of Messinian evaporites varies across the Mediterranean depending mainly on the tectonic setting and water depth. Four main settings are recognized. 1) Marginal zones with mainly erosional features (Fig. 3) that have commonly been related to multiple drawdown events[10,43] in which subaqueous erosion by dense cascading waters might also have played a role[44]. 2) Shallow, silled basins (Adriatic region, SE Spain basins) containing the most complete PLG successions[38], overlain in places by erosional surfaces and/or younger lacustrine and continental deposits with intervals characterized by brackish Lago Mare fauna[18,45–47]. 3) Intermediate-depth basins (Sicily, Cyprus, Balearic Promontory), which can be complicated by substantial tectonism during and since the MSC[23,48]. Basal MSC units in these intermediate settings comprise PLG[49] or anoxic shales devoid of evaporites[50,51]. Where PLG is observed, the evaporites

might not be preserved *in situ* because they are commonly found as a range of reworked deposits from gypsarenites to gypsum olistostromes, grouped into a Resedimented Lower Gypsum (RLG) unit[6,52].

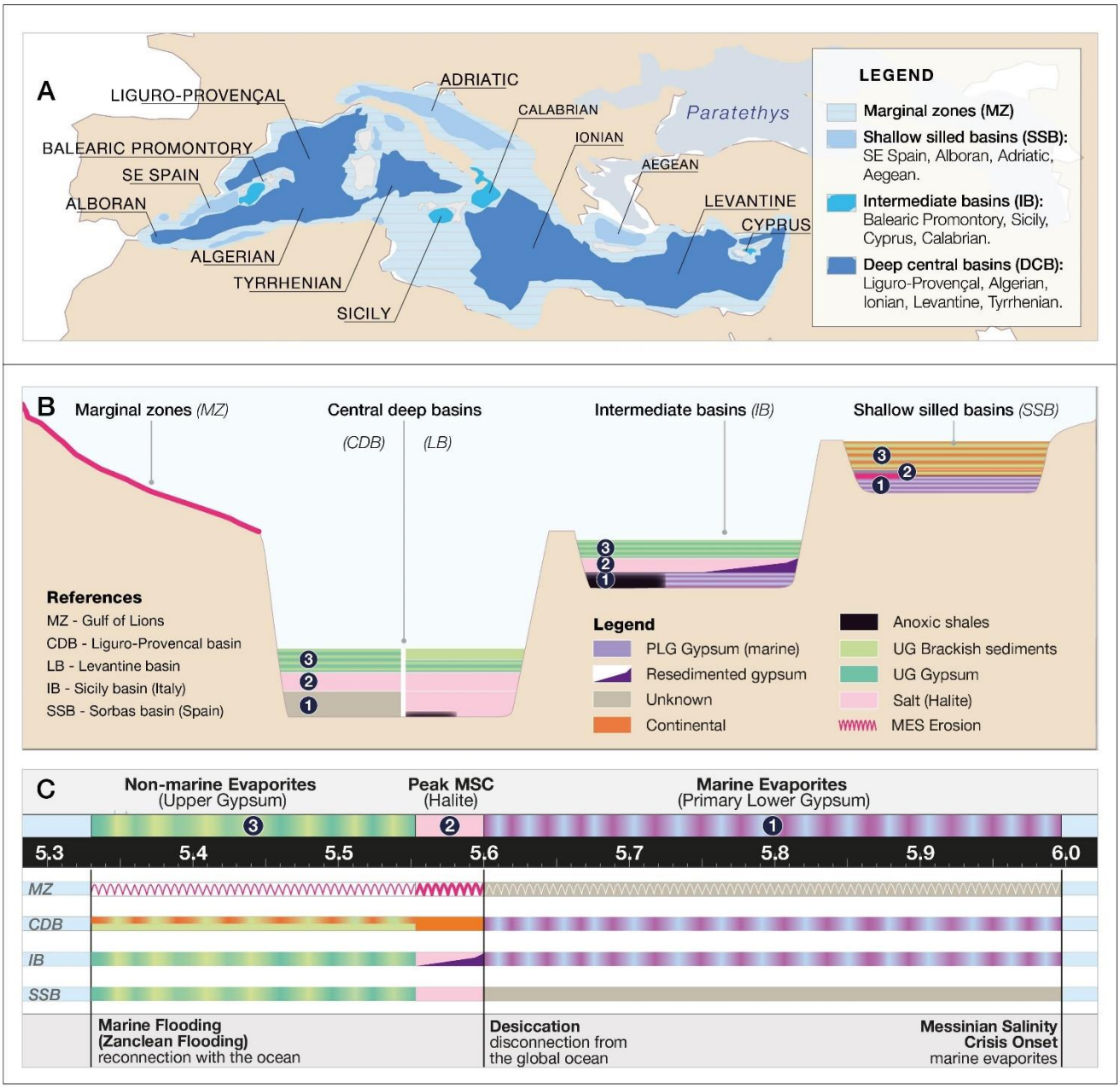

Figure 3. ***MSC stratigraphy in basinal settings.*** ***A*** *| Schematic Mediterranean map of Messinian marginal zones (MZ), shallow silled basins (SSB), intermediate basins (IB) and central deep basins (CDB).* ***B*** *| Schematic Mediterranean cross-section with MSC deposits in different basin settings. 1 Primary Lower Gypsum (PLG) phase, 2 Halite, 3 Upper Gypsum (UG) phase.* ***C*** *| Age constraints and distribution of MSC deposits in different basin settings.*

153 Downslope reworking is considered time-equivalent with the halite observed in intermediate-depth basins
154 (Sicily, Balearic Promontory, Cyprus)[23,53]. The UG is commonly well developed, comprising gypsum
155 alternating with clastics that contain Lago Mare fauna[18]. The transition from non-marine Messinian to deep
156 marine Zanclean deposits is often conformable without evidence of major erosion[54,55]. 4) Deep central basins
157 are found in the western (Liguro-Provençal, Algerian) and eastern (Ionian, Levantine) Mediterranean, separated
158 by the Strait of Sicily, with strikingly different depositional architecture on seismic refection profiles[7,10]. Deep
159 central western Mediterranean basins typically contain a seismic "trilogy" with a Lower Unit (mass-transport
160 deposits), Mobile Unit (halite), and an Upper Unit (gypsum-clastic alternations)[7]. No direct lithological data
161 are available for the deep central western salt giant where only the topmost MSC has been sampled, which
162 generally contains UG with brackish water fauna[56]. The easternmost deep Mediterranean (Levantine Basin)
163 contains a >1-km thick evaporitic succession with six seismic sub-units[57,58], four transparent units composed
164 of halite and two units composed of claystones[59,60]. Cuttings from industrial drill holes suggest that evaporite
165 deposition started with only a few metres of anhydrite[52,57], followed by the halite-dominated succession, which
166 terminated after a truncation surface with a ~100 m thick "Unit 7" composed of shales, sands, and anhydrite[9].
167 This top unit of the MSC in the deep Levant Basin is interpreted as having been deposited above the Intra
168 Messinian Truncation Surface (IMTS), a dissolution surface related to significant dilution and stratification of
169 the eastern Mediterranean water column at the base of the UG-Lago Mare phase[9].
170
171 ***Age constraints and hydrological conditions for Mediterranean evaporites***
172 Cyclostratigraphic correlation and astronomical tuning of pre- and post-MSC sedimentary successions provide
173 accurate ages for both the onset of PLG precipitation (5.97 Ma)[61], with evaporitic limestones in some
174 intermediate and marginal basins forming slightly earlier (6.08-6.03 Ma)[8,62,63], and the marine sediments that
175 immediately overlie the MSC successions throughout the Mediterranean (5.33 Ma)[64]. This constrains the MSC
176 duration to 640 kyr. Dating within the MSC interval itself is more uncertain because of a lack of high-resolution
177 independent age control points; the entire MSC occurred within a single reversed magnetic polarity

subchron[12,65] (Fig. 4); biostratigraphic markers are absent because of the extreme environmental conditions, and datable volcanic ash layers are scarce[6,46].

During the PLG phase, marine carbonate-marl and gypsum-marl cycles accumulated subaqueously in both shallow and intermediate basins (Fig. 3)[40], which precludes a major Mediterranean sea-level fall at the onset of the MSC[66]. Moreover, marine strontium isotope data are broadly consistent with a high Mediterranean water level that permitted restricted two-way Atlantic-Mediterranean exchange[15,67]. Assuming that cyclic gypsum-marl alternations followed the same regional precessional climate forcing as pre- and post-MSC Mediterranean sediments, correlation of 16-17 documented sedimentary cycles in the PLG to astronomical curves suggest that PLG deposition ended at <5.6 Ma (Fig. 4)[40,68]. However, numerical modelling of water and salt balances indicates

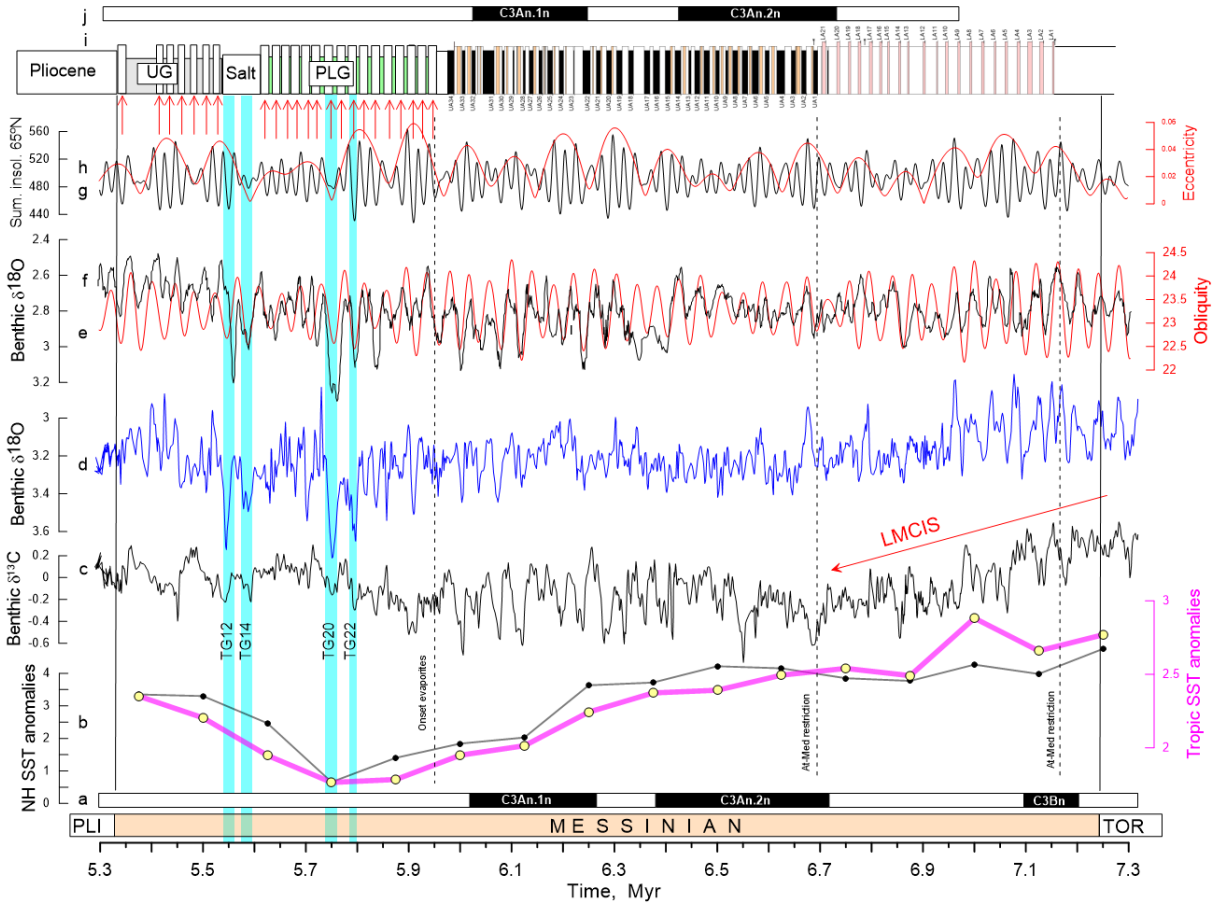

Figure 4. ***Global benthic foraminiferal oxygen and carbon isotope records correlated to the main MSC phases. a*** *| Cenozoic Geomagnetic Polarity Time Scale*[69,70]*.* ***b*** *| Northern Hemispheric sea surface temperature (SST) stack in black and Tropical sea surface temperature stack in magenta*[71]*. The scale shows the difference in temperature from the present (note that the two SST scales are different).* ***c*** *| Cenozoic benthic foraminiferal*

$\delta^{13}C$ reference record[69]*. LMCIS: Late Miocene Carbon Isotope Shift.* ***d*** *| Cenozoic benthic foraminiferal $\delta^{18}O$ reference record*[69]*.* ***e*** *| Changes in Earth´s tilt through the Messinian*[72]*.* ***f*** *| Benthic foraminiferal $\delta^{18}O$ from ODP Site 982 (North Atlantic)*[70]*.* ***g*** *| Insolation at 65°N for 21 June*[72]*.* ***h*** *| Changes in the Earth´s orbital eccentricity*[72]*.* ***i*** *| Messinian stratigraphic units. UG= Upper Gypsum, with 7 gypsum layers (white) interbedded with mudstones (grey)*[18]*, PLG=Primary Lower Gypsum with 16 gypsum layers (white) interbedded with mudstones*[6,21]*. Precession-driven sedimentary cycles during the pre-evaporite stage. LA1 to LA21 and UA1 to UA34 indicate Lower and Upper Abad sedimentary cycles*[13] *(the thickness of each sedimentary cycle has been adjusted to its time span)*[62]*. Legend for the pre-evaporite cycles: pink, white, black and beige levels indicate indurated layers, homogeneous marls, sapropels and diatomaceous marls, respectively.* ***j*** *| Geomagnetic polarity time scale GPTS2012*[73]*. Blue bands: main global glacial isotope stages during the Late Messinian. Dashed vertical lines: main restriction steps for Atlantic-Mediterranean water exchange; the upper one results in the PLG onset. Red arrows indicate gypsum beds deposited during insolation minima.*

that the gypsum-marl cycles could have resulted either from precession-driven ~20% hydrological budget changes and/or oscillating gateway restriction caused by sea-level fluctuations of ~10 m competing with tectonic uplift and marine gateway erosion[74,75] (Fig. 5).

Deep Mediterranean halite units lack absolute age control. In the western Mediterranean, halite is thought to have succeeded PLG deposition and is correlated tentatively with the TG12-14 glacial interval (5.59-5.55 Ma) in oxygen isotope ($\delta^{18}O$) records[21,76] (Figs. 4, 5). The timing of initial eastern Mediterranean halite deposition is contested, with suggested ages ranging from 5.97 Ma, equivalent to the PLG onset in marginal basins[77], to 5.59 Ma, at the end of the PLG[78]. Our sea-level analysis suggests a third possibility, namely ~5.8 Ma, which coincided with the start of glacial stage TG22 (Fig. 5). Halite is thought to have been deposited when Atlantic-Mediterranean exchange was more restricted than during the PLG phase[79] (see also *Methods*). In geochemical models, a severely restricted scenario with no Mediterranean outflow (that is, with Mediterranean sea level close to, or below, sill depth) could support deposition within 80 kyr of the deep-basin halite body observed in seismic profiles[79]. In this scenario, evaporated freshwater is replaced continuously by Atlantic inflow, which generates the necessary ion fluxes for halite deposition. The evaporite mineral paragenesis resulting from this constant marine supply with no ion loss via Mediterranean outflow is distinctly different from that generated by evaporation of a fixed seawater volume (Fig. 2). Instead of sequential evaporite phases precipitating as brine concentration increases, mineral precipitation fields overlap substantially, with carbonate, gypsum, and halite precipitation potentially coexisting up to bittern salt formation[80].

The final Mediterranean salt giant phase is the most enigmatic, with alternating UG beds and brackish Lago Mare deposits that contain biota of Paratethyan (former Black Sea-Caspian Sea system) affinity[46]. In intermediate basins (Sicily, Cyprus), 6-7 gypsum-brackish marl alternations are observed[21,81]. Strontium isotope ratios from both gypsum crystals in the UG and ostracods from Lago Mare marl horizons suggest a dominantly freshwater system with only minor (~20%) Atlantic contribution[18,42]. Assuming that UG cycles were precession-driven, downward tuning from the lowermost Zanclean suggests that this final MSC phase started at 5.52 Ma[18]. In shallow silled basins, time-equivalent continental and lacustrine sediments contain influxes of high-diversity Paratethyan ostracods, but no gypsum [45,82].

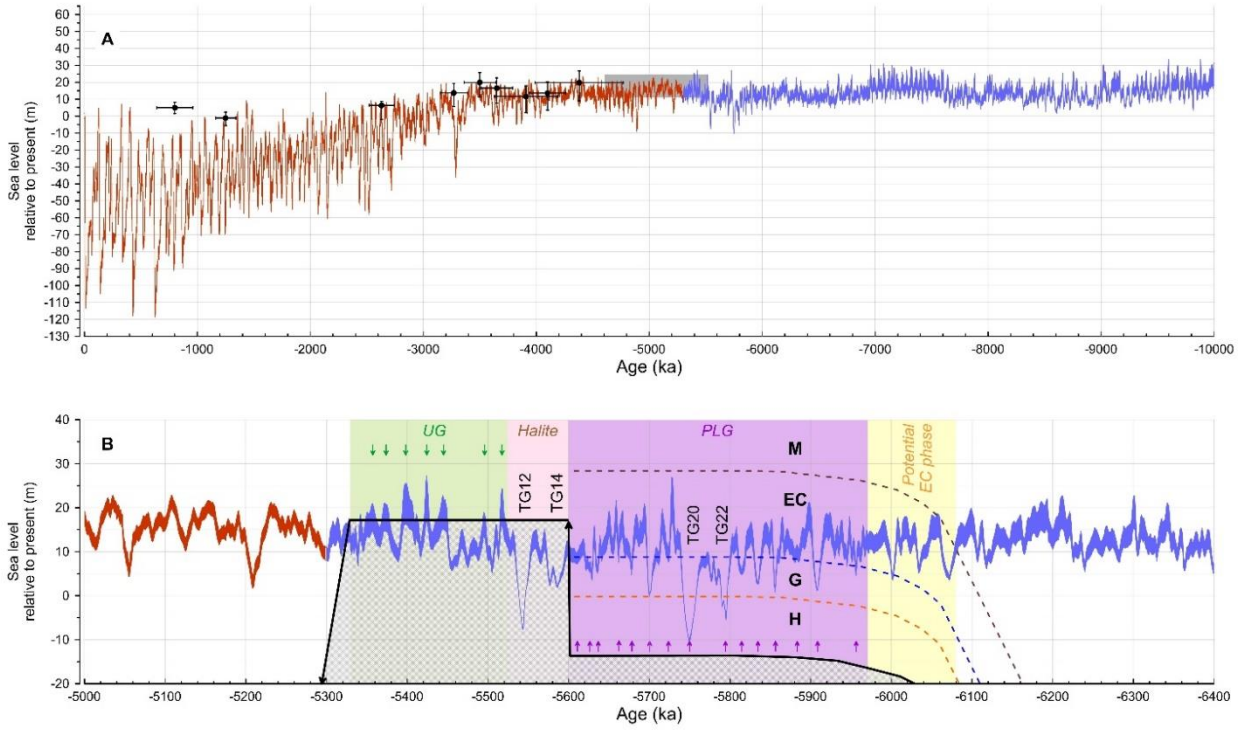

Figure 5. ***Sea-level synthesis with MSC sill-depth scenarios****.* ***a*** *| Last 10 Myr. The Plio-Pleistocene record (red) is based on benthic* $\delta^{18}O$ *deconvolution*[83,84] *using the combined compilations of Lisiecki and Raymo*[85] *and Westerhold et al.* [69]*. For the Miocene (blue), we use the envelope between the main benthic* $\delta^{18}O$ *deconvolution and the sensitivity scenario of Rohling et al.*[84] *(see that study for rationale and details) based on the Westerhold et al.*[69] *benthic* $\delta^{18}O$ *compilation. Sea-level benchmarks are also shown for Mallorcan marine cave deposits (black circles with error bars) and Patagonian coastal deposits (grey box), which have been corrected for tectonic changes, glacio-isostatic effects, and dynamic topography* [86–88]*.* ***b*** *| Detail of the records from* ***a*** *between 5 and 6.4 Ma. We compare sea-level variations with the likely Atlantic-Mediterranean gateway geometry and calculate threshold values for water exchange through the strait that delimit precipitation of halite (H), gypsum (G), evaporative carbonate (EC), or hemipelagic marl deposition (M), as detailed in the Methods. The inferred MSC sill (grey shading) scenario assumes a disconnected (drawn down) condition during halite and UG deposition. MSC phases are coloured as in Figure 3. Purple arrows indicate potential gypsum phases in the PLG, and green arrows indicate ~7 potential (mostly continental) gypsum phases in the UG.*

Salt giant forcing mechanisms: the roles of sills and straits

Marine gateways play a critical role in exchanging water, heat, salt, and nutrients between oceans and seas. During the MSC, water exchange with the open marine Atlantic Ocean and the brackish Paratethys Sea were influenced by a complex combination of geodynamic (tectonic movements in gateway regions), glacio-eustatic (global sea level fluctuations), and palaeoclimatic (hydrological budget changes) processes that all played a role in Messinian salt giant formation. Tectonic uplift and sea level lowering can have similar effects on water exchange through gateways and are difficult to unravel. Here, we present and evaluate current understanding of the geodynamic and ice-volume/sea-level forcings on the MSC and then revisit the role of superimposed regional palaeoclimatic forcing.

Geodynamic forcing

Salt giant formation requires the presence of a sill that restricts an evaporative basin from the open ocean. These sills generally form when continents collide or break apart by plate tectonic processes and provide the necessary raised lip across which exchange becomes restricted and allows development of water bodies with different chemical and physical properties. The strait at Gibraltar that connects the Mediterranean with the Atlantic is presently 284 m deep at the Camarinal sill and 14.3 km wide at the Tarifa narrows[89].

Palaeogeographic reconstructions of the Gibraltar region indicate that the early Messinian Atlantic-Mediterranean connection was a foreland-basin system with multiple gateways through southern Iberia and northern Morocco (Fig. 6a). These Betic and Rifian corridors closed progressively in pre-MSC times, and marine connectivity evolved toward a single proto-Gibraltar strait gateway for the MSC[22,90]. Mediterranean-Atlantic connectivity may also have been partially controlled by an emergent volcanic chain on the eastern Alborán margin that formed a partial land-bridge between northern Morocco and southeastern Spain (Fig. 6a)[91]. Water flux modelling indicates that exchange patterns with the Atlantic depended on relative sill depths, with two-way flow in two corridors when the shallow corridor was deeper than half the depth of the deep corridor, and only one-way flow when the shallow corridor was shallower than this[92]. Uplift of the initially deep Rifian

corridor at ~7 Ma[90] could, therefore, have altered exchange patterns in the Gibraltar strait from mainly Atlantic inflow to two-way flow, consistent with simultaneous Alborán Basin benthic faunal changes[93] and deep Mediterranean records in which the first signs of restricted conditions and increased water mass stratification occurred at ~7 Ma[94].

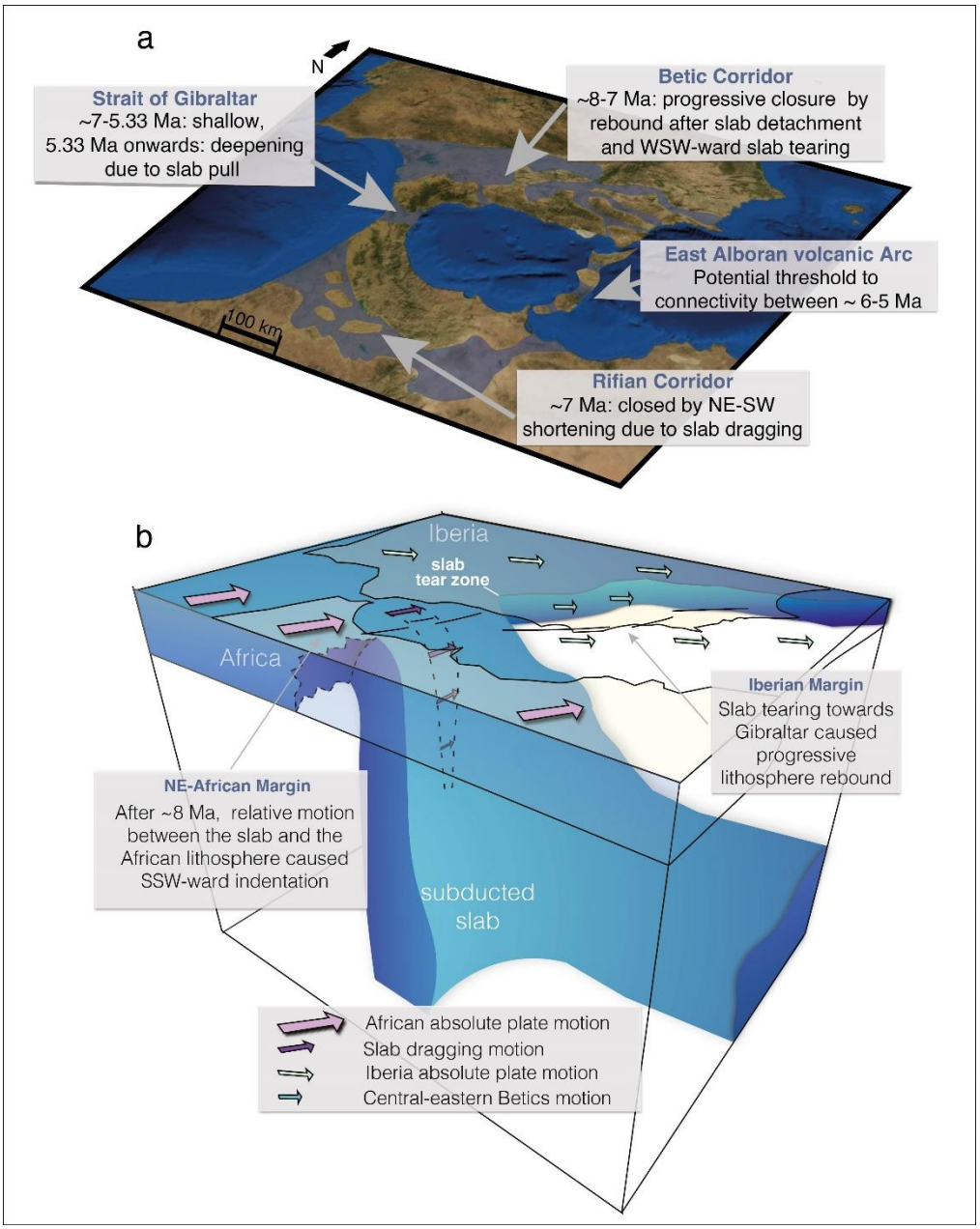

Figure 6. ***Geodynamic context of the MSC. a*** *| Schematic topography of the pre-MSC Gibraltar region with palaeogeographic projection of Mediterranean-Atlantic gateways. The labels illustrate the timing and mechanisms of vertical motion that restricted Atlantic-Mediterranean connectivity (~5.33–7 Ma) (after Capella et al.[95]).* ***b*** *| Cartoon of slab morphology below Gibraltar. Arrows illustrate absolute plate motions for Africa and Iberia with slower central-eastern Betic motion (after Spakman et al.[96]).*

The main geodynamic processes in the Gibraltar orogenic system involve African-Iberian plate convergence[97], slab tearing under the eastern Betic Cordillera[98], and mantle resistance against Gibraltar slab drag[96]. Mantle tomography and other seismological investigations provide a clear present-day 3D image of Gibraltar slab geometry and lateral continuity with surface plates, and where it is detached and might have delaminated from continental lithospheric mantle (Fig. 6b)[98,99]. Early to Late Miocene westward slab roll-back resulted in thrusting of the Alborán domain over the African and Iberian margins. Indentation of the Rif Mountains by slab dragging together with slab detachment beneath the Betic Cordillera (Fig. 6a, b) can explain gateway opening, closure, and re-opening[95]. During the late Tortonian (between 8 and 7 Ma), the Betic gateways were uplifted by isostatic rebound related to gradual slab tearing below Spain. Slab dragging initiated thick-skinned tectonics in Morocco that also closed the Rifian Corridor[100].

During the MSC, sills within the Mediterranean basin also played important roles. In shallow silled basins where PLG developed, geochemical evidence indicates that climate oscillations[101] modified conditions within the basins resulting in localised density contrasts across the sills, even before the MSC[102]. The Sicily sill, which separates the western and eastern Mediterranean basins, played a crucial role in water and salt transport across the Mediterranean before, during, and after the MSC[103–105], and likely generated the different MSC stratigraphies in the deep central basins. Other important sills were the tectonically active Gargano promontory (Italy)[106] and Cyclades region (Greece)[25] that separate, respectively, the Adriatic and North Aegean basins from the open eastern Mediterranean (Fig. 1). These restricted basins persisted as two evaporite-free largely isolated megalake systems during the halite and UG phases, probably influenced by extensive European river runoff (Fig. 1)[25,82].

In the eastern Mediterranean, the marine Neo-Tethys connection to the Indian Ocean had already closed in mid-Burdigalian times (~19-17 Ma), driven by Africa-Arabia/Eurasia collision[107,108], which created the first land bridge for mammal migration into and out of Africa. Consequently, this gateway probably played no role in Messinian salt giant evolution. Instead, the most important eastern connection during the MSC was with the Paratethys domain (Fig. 1). The present-day connection has sills 55 m deep and 1.2 km wide at the Dardanelles near Çanakkale, and 36 m deep and 698 m wide at the Bosporus near Istanbul[109] (Fig. 1a). Messinian

307 palaeogeographic evolution of the Mediterranean-Paratethys gateway is poorly understood, but it affected
308 hydrological, palaeoecological, and palaeoenvironmental conditions in both domains[25]. Palaeontological data
309 indicative of marine faunal exchange[110,111] and strontium isotope data[17] suggest that Mediterranean-Paratethys
310 connectivity was established at 6.1 Ma[112,113], before the onset of evaporite precipitation. Gateway geodynamics
311 between the Mediterranean and Paratethys were then, as now, dominated by active westward growth and
312 propagation of the North Anatolian Fault Zone, North Aegean extensional tectonics, and Cyclades domain
313 uplift/exhumation[114]. This, combined with substantial lake-level fluctuations, has resulted in episodic
314 Mediterranean-Paratethys/Black Sea connection and disconnection ever since[115,116].

315

316 ***Glacio-eustatic forcing***

317 To date, sea-level forcing of the MSC has been dismissed in most studies based on the assumption that its
318 variations were obliquity controlled (~40 kyr); using this period for sedimentary cyclicity would result in an
319 MSC duration that is too long to match independent age constraints. However, a recent global $\delta^{18}O$ synthesis
320 indicates that the periodicity of ice-volume and deep-sea temperature fluctuations across the Late Miocene was
321 controlled by precession, similar to Mediterranean climate cycles (Fig. 5)[69]. To assess whether sea level was
322 an important forcing mechanism for Mediterranean isolation from, and/or reconnection to, the Atlantic
323 Ocean[117], we examine a new sea-level record for the 6.4 to 5.0 Ma time interval relative to the present level (0
324 m; Fig. 5). By applying established box-model approaches to evaluate the evaporite implications of gateway
325 restriction[74] (see *Methods*), this sea-level record indicates that sill depths >41 m favour basinal hemipelagic
326 carbonate (marl) deposition. Evaporative carbonate deposition is favoured when the strait depth ranges between
327 22 and 41 m, gypsum deposition occurs between 13 and 22 m, and halite deposition occurs at depths <13 m.
328 Friction would reduce exchange through the strait, so these threshold water depths are minimum estimates.

329 The new high-resolution record of global mean sea-level variations indicates that sea level alone cannot account
330 for either the MSC onset, or rapid reestablishment of normal open marine conditions at the beginning of the
331 Pliocene. Tectonic strait restriction is needed to trigger the transition from open marine hemipelagites to
332 evaporative carbonates (6.08-6.03 Ma) followed by gypsum precipitation from 5.97 Ma (Fig. 5), while the

MSC termination requires catastrophic, tectonic, strait opening to depths more than ~40 m below the lowest sea level of that time[104,118]. However, some stratigraphic features within the MSC are consistent with Late Miocene sea level fluctuations. For example, with a shallow Mediterranean-Atlantic sill depth of 13-22 m (with the uplifted sill ~18 m below present-day sea level), sea-level fluctuations could explain the 16 gypsum cycles (magenta arrows in Fig. 5b) deposited during the PLG phase. In this scenario, sea-level influence on the gypsum cycles may have been irregular, potentially accounting for at least some observed variability in their thickness and spacing. These lithological threshold depth calculations ignore Paratethys inputs and precession-scale Mediterranean hydrologic budget fluctuations, which are likely to have varied; threshold depths will be somewhat smaller under more humid conditions and somewhat greater under more arid conditions (see[64] for sensitivity analysis). Changes in Paratethys inputs and Mediterranean hydrology might explain the absence of halite between 5.8 and 5.7 Ma, when it should have been triggered by two marked sea-level falls (Fig. 5b). The onset of well-documented halite precipitation (at ~5.6 Ma) requires further tectonic strait restriction (red shading in Fig. 5b). Maximum gateway restriction occurred at 5.55 Ma when global sea level was lowest, consistent with an episode of Mediterranean sea level fall. The end of halite deposition could have been terminated by the sea-level rise at ~5.53 Ma if the sill was below 6 m above present sea level.

For the UG phase (green shading in Fig. 5b), a (virtually) closed Atlantic connection with the basin in an essentially drawn-down state is required to obtain regional brackish to brine-water “lakes”, non-marine evaporite deposition, and continental-dominated Sr-isotope ratios[18,19,104]. This high-resolution sea-level record is consistent with (potentially seven) partial reconnection events (green arrows in Fig. 5b) associated with minor Atlantic inflow that might correspond to the seven gypsum cycles observed in the UG[18,81].

Palaeoclimate forcing

Salt giant formation requires an excess of evaporation over precipitation and runoff into the basin. These factors are difficult to quantify from geological records and reconstructions. For example, palaeo-runoff requires robust knowledge of the palaeogeographic evolution of the complete catchment area of an evaporite basin, including its orography and palaeo-channels. However, global climate models can provide some constraints[115–117]. We

here evaluate climatic variations over the Mediterranean basin and its catchment area, including the Paratethys and the north African monsoon region immediately before, during, and after the MSC.

Several records indicate that the Mediterranean salt giant formed during a period of global cooling between 7.2 and 5.5 Ma[70,71,119], which is likely to have been triggered by a global atmospheric pCO_2 decline to a minimum between 6.5 and 5.8 Ma[120]. The Late Miocene pCO_2 decrease has been linked to a ~1 ‰ global benthic foraminiferal $\delta^{13}C$ drop known as the Late Miocene Carbon Isotope Shift (LMCIS; Fig. 4) between 7.6 and 6.6 Ma[93,121]. This drop is amplified in the Mediterranean, probably because of progressive gateway restriction in the Gibraltar region since ~7.1 Ma[122]. The absence of a humidity decrease from the pre-evaporitic marls to the base of the PLG gypsum[92,122] implies that MSC salt giant formation was not likely triggered by Mediterranean climate change. As atmospheric pCO_2 began to rise after 5.5 Ma, warming occurred[120]. This warming trend started at the transition between isotope stages TG12 and TG11, coincident with the end of halite deposition and the onset of Mediterranean UG formation (Figs. 4, 5). Ensuing long-term global warming was associated with long-term global sea level rise (Figs. 4, 5)[83,84,117].

Lack of foraminifera hinders Mediterranean palaeoclimate reconstructions through the MSC, although Messinian palynological[123] and organic biomarker records[124–127] indicate that Mediterranean climate was warm and dry before, during, and after the MSC. Along the northern Mediterranean margin, climate was warm and humid, similar to present-day conditions, with important river runoff from the Alps (Rhone and Po)[128]. Lack of marked vegetation changes during the different evaporite phases suggests that Mediterranean climate did not force the MSC and that the MSC, in turn, did not have a substantial impact on Mediterranean climate[123].

The classic marl-sapropel alternations of pre-evaporitic MSC successions indicate conspicuous precession-paced climate oscillations (Fig. 4)[11,12,62], in which sapropels mark relatively wet conditions during precession minima (insolation maxima), when enhanced freshwater runoff increased Mediterranean water column stratification[129]. Whatever the role of eustatic sea-level variation, precessional forcing is assumed to have continued in the PLG deposits, with gypsum beds corresponding to relatively dry climates during precession maxima (insolation minima)[40,68]. Organic geochemical data from PLG cycles in northern Italy confirm this,

384 revealing climatic oscillations[15] with gypsum deposition during relatively dry periods with reduced river
385 runoff[130,131].

386 Most MSC scenarios envisage a maximum Mediterranean lowstand during or after halite deposition, with draw-
387 down estimates of -600 to -2000 m[43,132,133], indicating a strong regional circum-Mediterranean negative
388 hydrological balance. Mediterranean water level during the UG is still contested[46]. The presence of recurrent,
389 high-diversity, shallow-water, brackish ostracod assemblages in most shallow, silled Mediterranean basins
390 indicates considerable net freshwater influxes. Palaeoclimate models suggest that Mediterranean-wide Lago
391 Mare conditions cannot be explained by Paratethys inflow alone, and that additional water sources are
392 required[134,135]. Specifically, runoff from high-amplitude African monsoon maxima has been considered[136–140].
393 Alternatively, Atlantic input to the basin might have contributed during glacio-eustatic relative sea level
394 highstands (Fig. 5), although fully marine conditions were not established until the Zanclean[95].

395 Given Mediterranean regional hydroclimate constancy through the MSC, periods of strong evaporative water-
396 level drawdown must reflect low net precipitation over remote parts of the Mediterranean freshwater catchment
397 (Paratethys and/or monsoonal Africa). Conversely, major freshwater influx periods must reflect high net
398 precipitation over far reaches of its catchment. The Paratethys is a likely source of considerable Messinian
399 freshwater variations because connection between the two basins[110,136] would have greatly extended the
400 Mediterranean freshwater catchment area relative to today[19]. Specifically, the Messinian Paratethys unified the
401 Dacian, Black Sea, and Caspian Sea basins[105], so that all major Eurasian rivers (Danube, Dnjepr, Don, Volga,
402 Syr-Darya, Amu-Darya) drained into the Mediterranean[137]. In the Tortonian, hydrological variations associated
403 with eccentricity-driven northward (southward) mid-latitude westerly displacement over the Paratethys may
404 have already caused decreased (increased) Paratethys overspill/runoff into the Mediterranean[138]. Assuming that
405 similar climate variability continued through the Messinian and that it also had a precession-timed component,
406 the MSC net freshwater budget could have been affected substantially by Paratethys outflow[134,139].

407 African monsoon intensity tracked the northern summer insolation amplitude (hence the eccentricity-
408 modulated amplitude of the precession cycle) throughout much of the Neogene[140,141], including the MSC[142,143].
409 During insolation maxima (precession minima), monsoon-driven humidity expanded over north

410 Africa[140,141,144,145]. Large north African lakes, such as mega-lake Chad[135,139], might then have drained via the
411 ancient Eosahabi river into the Mediterranean[146–148]. Although lake Chad lies well south of the modern central
412 Saharan watershed, there is good evidence in younger geological periods of direct discharge via seasonal river
413 floods and wadis[149,150]. The absence of high-amplitude insolation maxima between 5.73 and 5.53 Ma suggests
414 an extended interval of relatively weak African monsoons, whereas several high-amplitude insolation maxima
415 during the UG phase suggest potential high-amplitude African monsoon maxima, with enhanced monsoon
416 runoff into the Mediterranean basin (Fig. 4).

417 Overall, it appears that the long-term evolution from pre-evaporitic marls to gypsum and salt deposition was
418 not driven predominantly by Mediterranean climate change, and that relative sea level drops interacting with
419 tectonic changes at gateways and their impact on ocean water exchange likely were the main mechanisms
420 leading to progressive salt concentration. This long-term trend was punctuated by both precession-based cycles
421 in sea-level and Mediterranean (including Paratethys and African monsoon) hydrology. The influence of these
422 astronomically driven variations was amplified progressively as Mediterranean restriction increased.
423

424 **Global relevance and future perspectives**

425 The Mediterranean MSC formed in a convergent tectonic setting. However, convergence is not complete, so it
426 is possible that the Messinian evaporites will, in time, represent merely the initial phase of salt giant formation
427 associated with ongoing Mediterranean basin closure. The MSC sequence contains deposits that provide
428 insights into both restriction and re-opening of a marginal sea (MSC onset and establishment of earliest
429 Pliocene marine conditions).

430 The MSC provides an illustration that salt giant formation is much more complex than simply evaporating a
431 sea water volume following its oceanic disconnection. The Messinian salt giant transitioned through three
432 restriction pheses from the open ocean (Fig. 1,3). First, restricted two-way exchange with maintained sea-level
433 connection between the Mediterranean and Atlantic resulted in gypsum precipitation with marine geochemical
434 signatures (PLG phase). Second, severely restricted oceanic inflow, sufficient to maintain evaporite ion flux
435 while Mediterranean sea-level fell, drove halite deposition. Third, extremely limited, intermittent oceanic

inflow led to continental-dominated, non-marine evaporite deposition alternating with brackish water conditions (UG phase). The sequence was terminated by abrupt reconnection and progressive restoration of normal marine conditions throughout the basin, re-establishing two-way Mediterranean-Atlantic exchange in the early Pliocene[18,104]. Return flux of MSC residual brine ions into the open ocean occurred over ~30,000 years[104] (Fig. 7) and its impacts on open ocean circulation and climate have yet to be investigated.

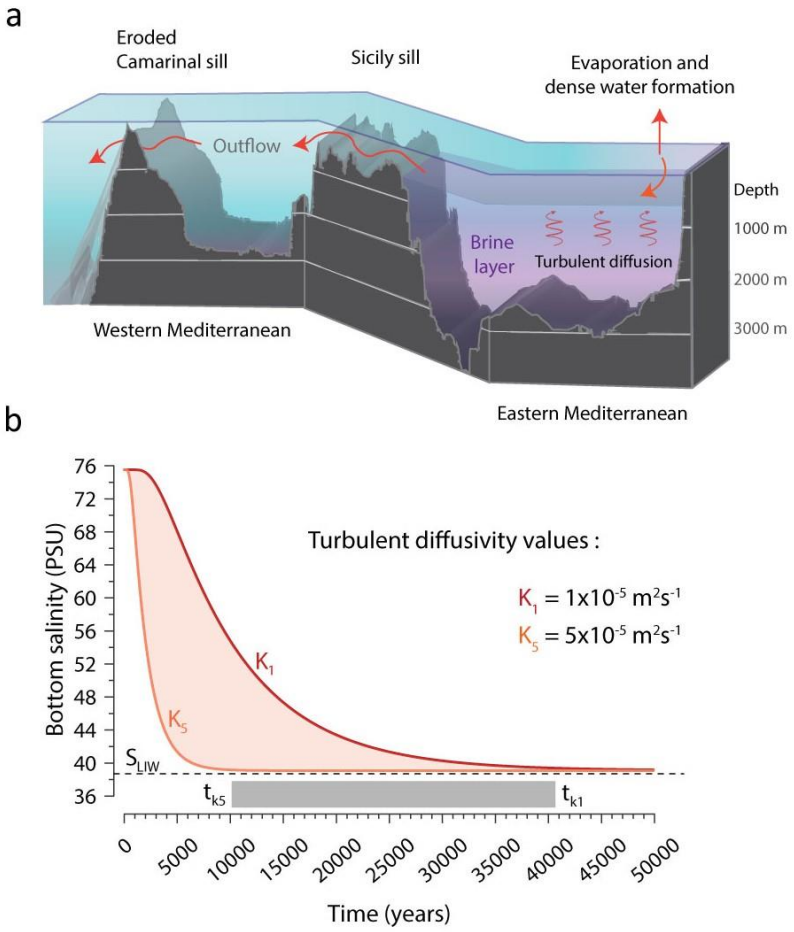

Figure 7. ***Post-MSC removal of Messinian salts to the Atlantic, following an abrupt refilling event. a*** *| Sketch of the Mediterranean configuration immediately following abrupt basin refilling by Atlantic waters. The energetic Atlantic inflow transferred almost all western Mediterranean Messinian salt to the Eastern basin, which became stratified with salts to the Sicily sill level. Turbulent diffusion of salts from the lower dense layer (driven by energy input from winds and tides) slowly transferred Messinian salts back to the Atlantic across the Sicily and Camarinal sills, via the outflow.* ***b*** *| Diagram of complete salt removal time scale (grey box: 10-40 kyr) for turbulent diffusivities of 1-5 × 10^{-5} m^2s^{-1}. The shaded area between the K_1 and K_5 curves represents all possible bottom water salinity reduction pathways. t_{k1}, t_{k5} = time taken to reach surface salinity values at K_1 and K_5 turbulent diffusivities. S_{LIW} = Levantine intermediate water salinity (after Amarathunga et al.[104]).*

Throughout all Mediterranean salt giant evaporitic phases, precession-timed runoff and/or global sea-level variations interacted to drive sedimentary environmental cyclicity due to greater/weaker freshwater admixtures and/or greater/weaker oceanic inflows to the basin, which overprinted marine connectivity changes due to tectonic gateway geometry changes. Model-based sensitivity tests indicate that even subtle freshwater budget and/or sea-level fluctuations would have sufficed to switch between gypsum and marl deposition[74]. Precession-timed arid/humid and precession-timed sea-level cycles both occurred at amplitudes relevant to the sedimentary regime, but the precise phase relationship between their impacts remains elusive; these processes could have partially amplified or cancelled each other. More advanced hydro-geochemical models that integrate both forcing mechanisms will be required to fully understand gypsum formation under restricted marine conditions. Hydro-geochemical modelling of salt giants can also provide useful information about the link between seawater-exchange restriction at the gateway sill and salinity evolution of the evaporite basin[67,79,105]. These models track salinity as a single variable, or at most divide salinity into three contributions: gypsum (Ca and SO_4), halite (Na and Cl), and other salts (K, Mg, HCO_3^-). This simplification, which facilitates numerical model solution, comes at the expense of a more correct thermodynamic description of the brine and its evolution during salt giant formation.

The exact drawdown amount remains a key unknown regarding halite and non-marine gypsum precipitation, when the evaporite basin was semi-isolated from the ocean. Maximum lowstands based on seismic interpretations combined with numerical modelling differ between -600 and -2000 m, assuming that all observed Messinian erosional surfaces formed subaerially. At times of severely restricted or negligible Atlantic inflow, Mediterranean evaporites are expected to contain a mineralogical imprint of continental runoff. The low Ca^{2+}/Cl^- and SO_4^{2-}/Cl^- in continental runoff enables gypsum precipitation at much lower salinities than when forming from evaporating seawater[17,31]. Future hydro-geochemical models that integrate a sound thermodynamic description of high-salinity brines[80] will be able to test the hypothesis that increased relative importance of riverine inputs produces a substantial mineralogical assemblage change in a salt giant. Such models can also evaluate if a large (> 1.5 km) drawdown is required to attain brine saturation with respect to the highly soluble mineral bischofite, which is known to have precipitated during the MSC based on pore water

477 geochemical tracers measured from the *Discovery*, *Hephaestus*, and *Kryos* deep-sea hypersaline lakes on the
478 Mediterranean Ridge[151–153].

479 Almost all salt giant-related research to date has focused on their nature and causes[6,154] with little consideration
480 of their potential to drive wider environmental change[18,155]. This is partly because of an assumption that impacts
481 outside the salt basin will be synchronous with evaporite formation. Some recent MSC research has challenged
482 that assumption [18,155] and in doing so, has initiated new research into the chemical and physical consequences
483 of the MSC and salt giants more generally for regional and global climate.

484 While the impact of evaporite formation and subsequent weathering on ocean chemistry has been known for
485 some time[162], their potential to drive rapid carbon cycle changes and associated climate change has only recently
486 been pointed out[155]. Modelling of evaporite weathering and deposition suggests that despite the much larger
487 halite volume that is typically preserved in salt giants, it is the formation and dissolution of giant calcium
488 sulphate (gypsum/anhydrite) deposits that can have global consequences as an episodic driver of carbon cycle
489 changes[155]. This is because oceanic Ca^{2+} removal via $CaSO_4$ deposition decouples the oceanic Ca^{2+} and HCO_3^-
490 sinks, causing a $CaCO_3$ burial decrease and, consequently, increased ocean pH, lower atmospheric pCO_2, and
491 global cooling. Similarly, the return of Ca^{2+} ions to the ocean from weathered gypsum can drive warming[155].

492 Most biogeochemical models have ignored evaporite-driven perturbations to seawater chemistry[156,157],
493 assuming that over timescales >100 kyr, evaporite precipitation and weathering are balanced. Formation of
494 substantial MSC evaporites, and their preservation over the subsequent ~5 million years of Earth history,
495 reflects a ~7 to 10 % net evaporite-ion extraction from ocean water over this period[4,39]. Bearing in mind that
496 the MSC is by no means the largest of the salt giants[158], this demonstrates that the evaporite precipitation-
497 weathering balance assumption can only be true on multi-million year timescales at best, and suggests that
498 current carbon cycle models may be missing an important intermediate timescale climatic driver[155].

499 Initial sensitivity experiments that explored the impact of gypsum precipitation/weathering on the carbon cycle,
500 recognised that the precipitation and preservation of any gypsum represents a net reduction in oceanic $[Ca^{2+}]$
501 and expressed this as a constant Ca^{2+} forcing[155] for the duration of salt giant formation. However, in detail the

502 Ca^{2+} ion flux associated with a salt giant is not constant, but far more complex, reflecting cyclic evaporite
503 formation and the evolving connectivity history of the salt-bearing basin. For the MSC, this means that during
504 the PLG, when gypsum-marl alternations formed under conditions of two-way Atlantic-Mediterranean
505 exchange, Ca^{2+} ion loss from the global ocean occurred episodically, reflecting each precipitation event[18]. It is
506 also likely that return flux to the global ocean occurred as the newly formed gypsum layers partially dissolved[18].
507 This return flux cannot have occurred during the later MSC stages, when there was no Mediterranean outflow.
508 Any ions liberated by exposure and weathering of evaporites during periods of lowered Mediterranean sea level
509 would have remained trapped within the basin at least until early Pliocene reestablishment of two-way exchange
510 and flushing of residual brines which took ~30,000 years[104]. New model simulations that incorporate realistic
511 Ca^{2+} ion flux records are, therefore, required to evaluate the magnitude of any evaporite-driven climate
512 perturbation.

513 Reconstructing the magnitude and timing of evaporite ion fluxes, however, is challenging. The salt volume
514 preserved today is not a robust measure of the total evaporite ions extracted, but rather represents a minimum
515 value for what was originally precipitated. Additional evaporites may have been precipitated and dissolved
516 either before burial or during later exposure by orogenic processes[5]. Evaporite minerals also precipitate and
517 dissolve three orders of magnitude more rapidly than other sediments[159]. Consequently, their impact on the
518 carbon cycle can be an order of magnitude quicker than the carbonate-silicate weathering feedback[155]. Through
519 burial, evaporites can also be stored in rock successions for long periods outside the ocean-climate system[25].
520 As a result, evaporite-mediated ion extraction from, and return to, the ocean can be both rapid (10^3-10^4 y),
521 occurring during or shortly after salt giant formation, as is largely the case for the MSC, and/or gradual ($>>10^6$
522 y) where dissolution occurs post burial, as is occurring in Arctic Canada where a ~290-million-year-old gypsum
523 salt giant is now emerging from beneath thawing and eroding permafrost[160].

524 Constraints on the evaporite-ion flux in addition to the salt giant succession itself are clearly required. One
525 possibility is to use the seawater [Ca^{2+}] record[161]. To capture perturbations anticipated from salt giant formation,
526 a high-resolution record is required. However, currently only a handful of [Ca^{2+}] measurements exist for the
527 entire Cenozoic (ironically mainly from evaporite fluid inclusions[161]). These reveal a general decline over the

past 100 million years[161], but are too few to detect a net $[Ca^{2+}]_{sw}$ reduction over the MSC duration, let alone the abrupt sub-precessional scale step-like structure that should be evident from evaporite ion extraction and return. By integrating Ca-evaporite formation and weathering processes, coupled carbon and calcium cycle models will provide more mechanistically sound explanations of the links between geological and geochemical cycles, and climate.

Physical processes associated with salt giant formation may also have a potential impact on global climate. Advection of dense, cold/salty overflow water from marginal basins strongly influences the oceanic distribution of heat and salt, exerting a powerful influence on thermohaline circulation and deep-water formation[162]. In the North Atlantic today, the densest of these overflows emanates from the Mediterranean Sea[163] depositing a prominent overflow plume that contours around the Iberian margin[164]. Sensitivity experiments that exclude present-day Mediterranean-Atlantic exchange result in ~1° cooling over the North Atlantic, and a 0.7-2.3 Sv (1 Sv=10^6 m^3/s) reduction in the Atlantic Meridonal Overturning Circulation[162,165]. These results indicate that the negative Mediterranean hydrologic budget, combined with exchange through the Gibraltar Strait, is enough to generate a climatically important high-density water mass today. The outstanding question is: what role did this overflow play in driving Late Miocene climate?

Mediterranean overflow was triggered by initial tectonic restriction of Mediterranean-Atlantic exchange as the two pre-Gibraltar marine gateways formed and closed, allowing a Mediterranean-Atlantic density contrast to develop[166]. This restriction process occurred at ~8 Ma[166] (Fig. 6a), and pre-dated evaporite deposition by two million years and persisted after the MSC throughout the Pliocene and Pleistocene[164]. Similar dense overflows may be associated with every marginal basin in which a salt giant has formed and, like the MSC, their duration will not have been synchronous with salt giant formation. The impact of these overflows on thermohaline circulation has yet to be explored.

During salt giant formation, marginal basin water density will have been much higher, and evaporite-sediment alternations such as those of MSC successions, indicate fluctuating brine concentrations. However, only during two-way exchange episodes will this produce a high-density overflow plume that could impact thermohaline circulation. Modelling these extreme high-density overflows is challenging because the narrow, shallow marine

554 gateways required for overflows to form are too small to be fully resolvable in current Earth System Models.
555 Instead, models use various parameterisations to mimic overflow mixing in model simulations[167,168]; none are
556 currently compatible with densities that far exceed contemporary overflow observations[163]. Improved model
557 parameterisation of overflow mixing and development of proxies that allow overflow density reconstruction
558 will be critical to addressing this challenge.

559 Finally, this review provides context for the upcoming Land-2-Sea drilling project, IMMAGE (Investigating
560 Miocene Mediterranean-Atlantic Gateway Exchange)[169], which involves both offshore drilling with
561 International Ocean Discovery Program Expedition 401 on either side of the Gibraltar Strait and onshore
562 drilling with the International Continental Scientific Drilling Program in Morocco and Spain, targeting the two
563 precursor Atlantic-Mediterranean marine connections that have been uplifted and preserved on land. IMMAGE
564 will recover 8-4 million-year-old sediments from both gateways and the Mediterranean outflow plume in the
565 Atlantic before, during, and after the MSC. The objective is to identify and quantify the impact of evolving
566 Mediterranean-Atlantic exchange on regional and global environmental change and specifically its potential
567 contribution to cooling during this period, which ultimately resulted in initiation of northern hemisphere
568 glaciation[71]. IMMAGE, the first Land-2-Sea drilling project, offers great scope for addressing many remaining
569 unknowns outlined here.

570

571 **Methods**

572 We constructed a sea-level record relative to the present level (0 m) for the 7.5 to 5.0 Ma time interval from
573 the synthesis of Rohling et al.[84]. We include sea-level benchmarks from Mallorcan marine cave deposits and
574 Patagonian coastal deposits, which have been corrected for tectonic changes, glacio-isostatic effects, and
575 dynamic topography[86–88], and which corroborate the sea-level record from benthic $\delta^{18}O$ deconvolution before,
576 and across, the Miocene-Pliocene boundary. Water exchange thresholds were calculated using the channel
577 geometries of Krijgsman et al.[22], which we combine into an approximately triangular single width vs. depth
578 profile (maximum width = 3.28 km; maximum depth = 136 m). Today, the Gibraltar Strait is 10.67 km wide at
579 sea level with 136 m of water above the sill. Hence, the triangular cross-sectional area of the Messinian strait
580 was 3.25 times more restricted than the modern triangular cross-sectional strait area for the same depth. We
581 use this extra restriction in the Bryden and Kinder[170] model for water exchange through the strait, ignoring

friction and assuming that excess evaporation (= evaporation − precipitation – runoff) over the basin was equal to that at present. We then calculate water depths in the Messinian strait required for key basin salinity thresholds of 350 (halite), 135 (gypsum), and ~75 ppt (evaporative carbonate); this yields depths of 13 m, 22 m, and 41 m, respectively.

Acknowledgements

This research was supported by the project SALTGIANT-Understanding the Mediterranean Salt Giant, funded by the European Union's Horizon 2020 program (Marie Skłodowska-Curie grant agreement No 765256). It also contributes to Australian Research Council projects FL120100050, DP2000101157 (E.J.R.), and DP190100874 (A.P.R.), and Veni grant 212.136 (D.V.P.) financed by the Dutch Research Council (NWO).

Competing interests

The authors declare that they have no known competing financial interests or personal relationships that could have appeared to influence the work reported in this paper.

Author contributions

All authors contributed to the content, discussion, writing, and editing of the paper. DP, FR, VA, FS, EJR, and UA constructed the figures.

References

1. Camerlenghi, A. & Aloisi, V. Uncovering the Mediterranean salt giant (MEDSALT) - scientific networking as incubator of cross-disciplinary research in Earth sciences. *Eur. Rev.* **28**, 40–61 (2020).
2. Hübscher, C. *et al.* Global look at salt giants. *Eos (Washington DC)* **88**, (2007).
3. Ryan, W. B. F. Decoding the Mediterranean salinity crisis. *Sedimentology* **56**, 95–136 (2009).
4. Haq, B., Gorini, C., Baur, J., Moneron, J. & Rubino, J. Deep Mediterranean's Messinian evaporite giant: how much salt ? *Glob. Planet. Change* **184**, 103052 (2020).
5. Wortmann, U. & Paytan, A. Rapid variability of seawater chemistry over the past 130 million years. *Science* **337**, 334–336 (2012).
6. Roveri, M. *et al.* The Messinian Salinity Crisis: past and future of a great challenge for marine sciences. *Mar. Geol.* **352**, 25–58 (2014).
7. Lofi, J. *et al.* Erosional processes and paleo-environmental changes in the Western Gulf of Lions (SW France) during the Messinian Salinity Crisis. *Mar. Geol.* **217**, 1–30 (2005).
8. Rouchy, J. M. & Caruso, A. The Messinian salinity crisis in the Mediterranean basin: A reassessment of the data and an integrated scenario. *Sediment. Geol.* **188–189**, 35–67 (2006).
9. Gvirtzman, Z. *et al.* Intra-Messinian truncation surface in the Levant Basin explained by subaqueous dissolution. *Geology* **45**, 915–918 (2017).
10. Lofi, J. *et al.* Refining our knowledge of the Messinian salinity crisis records in the offshore domain through multi-site seismic analysis. *Bull Soc. Geol.France* **182**, 163–180 (2011).
11. Hilgen, F. J. *et al.* Extending the astronomical (polarity) time scale into the Miocene. *Earth Planet. Sci. Lett.* **136**, 495–510 (1995).
12. Krijgsman, W., Hilgen, F. J., Raffi, I., Sierro, F. J. & Wilson, D. S. Chronology, causes and progression of the Messinian salinity crisis. *Nature* **400**, 652–655 (1999).

13. Sierro, F. J., Hilgen, F. J., Krijgsman, W. & Flores, J. A. The Abad composite (SE Spain): a Messinian reference section for the Mediterranean and the APTS. *Palaeogeogr. Palaeoclimatol. Palaeoecol.* **168**, 141–169 (2001).
14. Natalicchio, M. *et al.* Did late Miocene (Messinian) gypsum precipitate from evaporated marine brines? Insights from the Piedmont basin (Italy). *Geology* **42**, 179–182 (2014).
15. Reghizzi, M., Lugli, S., Manzi, V., Rossi, F. P. & Roveri, M. Orbitally forced hydrological balance during the Messinian Salinity Crisis: Insights from strontium isotopes (87Sr/86Sr) in the Vena del Gesso Basin (Northern Apennines, Italy). *Paleoceanogr. Paleoclimatol.*.**33**, 716–731 (2018).
16. Topper, R. P. M. & Meijer, P. T. A modeling perspective on spatial and temporal variations in Messinian evaporite deposits. *Mar. Geol.* **336**, 44–60 (2013).
17. Grothe, A. *et al.* Paratethys pacing of the Messinian Salinity Crisis : low salinity waters contributing to gypsum precipitation? *Earth Planet. Sci. Lett.* **532**, 116029 (2020).
18. Andreetto, F. *et al.* High-amplitude water-level fluctuations at the end of the Mediterranean Messinian Salinity Crisis: implications for gypsum formation, connectivity and global climate. *Earth Planet. Sci. Lett.* **595**, 117767 (2022).
19. Raad, F. *et al.* A song of volumes, surfaces and fluxes: the case study of the Central Mallorca Depression (Balearic Promontory) during the Messinian Salinity Crisis. *Basin Res.* **35**, 1–27 (2023).
20. Flecker, R. *et al.* Evolution of the Late Miocene Mediterranean-Atlantic gateways and their impact on regional and global environmental change. *Earth Sci. Rev.* **150**, 365–392 (2015).
21. Hilgen, F., Kuiper, K., Krijgsman, W., Snel, E. & Van der Laan, E. Astronomical tuning as the basis for high resolution chronostratigraphy : the intricate history of the Messinian Salinity Crisis. *Stratigraphy* **4**, 231–238 (2007).
22. Krijgsman, W. *et al.* The Gibraltar Corridor: Watergate of the Messinian Salinity Crisis. *Mar. Geol.* **403**, 238–246 (2018).
23. Raad, F., Lofi, J., Maillard, A., Tzevahirtzian, A. & Caruso, A. The Messinian Salinity Crisis deposits in the Balearic Promontory: an undeformed analog of the MSC Sicilian basins?? *Mar. Pet. Geol.* **124**, 104777 (2021).
24. Popov, S. V. *et al.* Late Miocene to Pliocene palaeogeography of the Paratethys and its relation to the Mediterranean. *Palaeogeogr. Palaeoclimatol. Palaeoecol.* **238**, 91–106 (2006).
25. Krijgsman, W., Palcu, D. V., Andreetto, F., Stoica, M. & Mandic, O. Changing seas in the late Miocene Northern Aegean: a Paratethyan perspective to Mediterranean stratigraphy. *Earth Sci. Rev.* **210**, 103386 (2020).
26. Lowenstein, T. K., Timofeeff, M. N., Brennan, S. T., Hardie, L. A. & Demicco, R. V. Oscillations in Phanerozoic seawater chemistry: evidence from fluid Inclusions. *Science* **294**, 1086–1088 (2001).
27. Bąbel, M. & Schreiber, B. C. *Geochemistry of Evaporites and Evolution of Seawater*. *Treatise on Geochemistry: Second Edition* vol. 9 (2014).
28. Harvie, C. E. & Weare, J. H. The prediction of mineral solubilities in natural waters: the Na-K-Mg-Ca-Cl-$S0_4$-H_2O system from zero to high concentration at 25°C. *Geochim Cosmochim Acta* **44**, 723–751 (1980).
29. Gaillardet, J., Dupré, B., Louvat, P. & Allègre, C. J. Global silicate weathering and CO2 consumption rates deduced from the chemistry of large rivers. *Chem Geol* **159**, 3–30 (1999).
30. Meybeck, M. Global analysis of river systems: from Earth system controls to Anthropocene syndromes. *Phil. Tran. R. Soc.Lond.* **358**, 1935–1955 (2003).
31. Aloisi, G. *et al.* The geochemical riddle of "low-salinity gypsum" deposits. *Geochim. Cosmochim. Acta* **327**, 247–275 (2022).
32. Selli, R. Il Messiniano Mayer-Eymar 1867. Proposta di un neostratotipo. *Giornale di Geologia* **28**, 1–33 (1960).
33. Ruggieri, G. The Miocene and later evolution of the Mediterranean Sea. *Aspects of Tethyan Biogeography* 283–290 (1967).
34. Hsü, K., Ryan, W. B. F. & Cita, M. Late Miocene desiccation of the Mediterranean. *Nature* **242**, 240–244 (1973).
35. Ryan, W. B. F. 50th anniversary review of the Mediterranean desiccation hypothesis. *Rivista del Nuovo Cimento* **46** 163 (2023).
36. Manzi, V., Lugli, S., Roveri, M., Schreiber, B. C. & Gennari, R. The Messinian 'Calcare di Base' (Sicily, Italy) revisited. *Bull. Geol. Soc. Am.* **123**, 347–370 (2011).
37. Caruso, A., Pierre, C., Blanc-Valleron, M.-M. & Rouchy, J. M. Carbonate deposition and diagenesis in evaporitic environments: the evaporative and sulphur-bearing limestones during the settlement of the Messinian Salinity Crisis in Sicily and Calabria. *Palaeogeogr. Palaeoclimatol. Palaeoecol.* **429**, 136–162 (2015).
38. Bourillot, R. *et al.* Structure and evolution of a Messinian mixed carbonate-siliciclastic platform: the role of evaporites (Sorbas Basin, South-East Spain). *Sedimentology* **57**, 477–512 (2010).

39. Roveri, M., Lugli, S., Manzi, V., Reghizzi, M. & Rossi, F. P. Stratigraphic relationships between shallow-water carbonates and primary gypsum: insights from the Messinian succession of the Sorbas Basin (Betic Cordillera, Southern Spain). *Sediment. Geol.* **404**, 105678 (2020).
40. Lugli, S., Manzi, V., Roveri, M. & Schreiber, B. C. The Primary Lower Gypsum in the Mediterranean: a new facies interpretation for the first stage of the Messinian salinity crisis. *Palaeogeogr. Palaeoclimatol. Palaeoecol.* **297**, 83–99 (2010).
41. Manzi, V. *et al.* High-frequency cyclicity in the Mediterranean Messinian evaporites: evidence for solar-lunar climate forcing. *J. Sed. Res.* **82**, 991–1005 (2012).
42. García-Veigas, J., Cendón, D. I., Gibert, L., Lowenstein, T. K. & Artiaga, D. Geochemical indicators in Western Mediterranean Messinian evaporites: Implications for the salinity crisis. *Mar. Geol.* **403**, 197–214 (2018).
43. Heida, H. *et al.* Flexural-isostatic reconstruction of the Western Mediterranean during the Messinian Salinity Crisis: implications for water level and basin connectivity. *Basin Res.* **34**, 50–80 (2022).
44. Roveri, M. *et al.* Dense shelf water cascading and Messinian Canyons: a new scenario for the Mediterranean salinity crisis. *Am. J. Sci.* **314**, 751–784 (2014).
45. Stoica, M., Krijgsman, W., Fortuin, A. & Gliozzi, E. Paratethyan ostracods in the Spanish Lago-Mare: more evidence for interbasinal exchange at high Mediterranean sea level. *Palaeogeogr. Palaeoclimatol. Palaeoecol.* **441**, 854–870 (2016).
46. Andreetto, F. *et al.* Freshening of the Mediterranean Salt Giant: controversies and certainties around the terminal (Upper Gypsum and Lago-Mare) phases of the Messinian Salinity Crisis. *Earth Sci. Rev.* **216**, 103577 (2021).
47. Gliozzi, E., Ceci, M. E., Grossi, F. & Ligios, S. Paratethyan ostracod immigrants in Italy during the Late Miocene. *Geobios* **40**, 325–337 (2007).
48. Manzi, V., Lugli, S., Ricci Lucchi, F. & Roveri, M. Deep-water clastic evaporites deposition in the Messinian Adriatic foredeep (northern Apennines, Italy): did the Mediterranean ever dry out? *Sedimentology* **52**, 875–902 (2005).
49. Ochoa, D. *et al.* Messinian Salinity Crisis deposits widespread over the Balearic Promontory : Insights from new high-resolution seismic data. Mar. Pet. Geol. **66** 41–54 (2014)
50. Manzi, V. *et al.* The deep-water counterpart of the Messinian Lower Evaporites in the Apennine foredeep: the Fanantello section (Northern Apennines, Italy). *Palaeogeogr. Palaeoclimatol. Palaeoecol.* **251**, 470–499 (2007).
51. de Lange, G. J. & Krijgsman, W. Messinian salinity crisis: a novel unifying shallow gypsum/deep dolomite formation mechanism. *Mar. Geol.* **275**, 273–277 (2010).
52. Manzi, V., Roveri, M., Argnani, A., Cowan, D. & Lugli, S. Large-scale mass-transport deposits recording the collapse of an evaporitic platform during the Messinian salinity crisis (Caltanissetta basin, Sicily). *Sediment. Geol.* **424**, 106003 (2021).
53. Roveri, M., Lugli, S., Manzi, V. & Schreiber, B. C. The Messinian Sicilian stratigraphy revisited: new insights for the Messinian salinity crisis. *Terra Nova* **20**, 483–488 (2008).
54. Bulian, F., Kouwenhoven, T. J., Andersen, N., Krijgsman, W. & Sierro, F. J. Reflooding and repopulation of the Mediterranean Sea after the Messinian Salinity Crisis: benthic foraminifera assemblages and stable isotopes of Spanish basins. *Mar. Micropaleontol.* **176**, 102160 (2022).
55. van Dijk, G. *et al.* A terminal Messinian flooding of the Mediterranean evidenced by contouritic deposits on Sicily. *Sedimentology* **70**, 1195–1223 (2023).
56. Lugli, S., Manzi, V., Roveri, M. & Schreiber, B. C. The deep record of the Messinian salinity crisis: evidence of a non-desiccated Mediterranean Sea. *Palaeogeogr. Palaeoclimatol. Palaeoecol.* **433**, 201–218 (2015).
57. Gvirtzman, Z., Reshef, M., Buch-Leviatan, O. & Ben-Avraham, Z. Intense salt deformation in the Levant Basin in the middle of the Messinian Salinity Crisis. *Earth Planet. Sci. Lett.* **379**, 108–119 (2013).
58. Bertoni, C. & Cartwright, J. A. Controls on the basinwide architecture of late Miocene (Messinian) evaporites on the Levant margin (Eastern Mediterranean). *Sediment. Geol.* **188–189**, 93–114 (2006).
59. Feng, Y. E., Steinberg, J. & Reshef, M. Intra-salt deformation: implications for the evolution of the Messinian evaporites in the Levant Basin, eastern Mediterranean. *Mar. Pet. Geol.* **88**, 251–267 (2017).
60. Feng, Y. E., Yankelzon, A., Steinberg, J. & Reshef, M. Lithology and characteristics of the Messinian evaporite sequence of the deep Levant Basin, Eastern Mediterranean. *Mar. Geol.* **376**, 118–131 (2016).
61. Manzi, V. *et al.* Age refinement of the Messinian salinity crisis onset in the Mediterranean. *Terra Nova* **25**, 315–322 (2013).
62. Zachariasse, W. J. & Lourens, L. J. The Messinian on Gavdos (Greece) and the status of currently used ages for the onset of the MSC and gypsum precipitation. *Newsl. Stratigr.* **55**, 333–360 (2022).
63. Tzevahirtzian, A., Caruso, A., Andreetto, F., Bonomo, S. & Krijgsman, W. A bio-chronostratigraphic study of the upper Miocene from the northern Caltanissetta Basin, Sicily (core 3AGN2S04). implications for dating the Messinian Salinity Crisis onset. *Sediment. Geol.* **445**, (2023).

64. Van Couvering, J. A., Castradori, D., Cita, M. B., Hilgen, F. J. & Rio, D. The base of the Zanclean Stage and of the Pliocene Series. *Episodes* **23**, 179–187 (2000).
65. Clauzon, G., Suc, J.-P., Gautier, F., Berger, A. & Loutre, M.-F. Alternate interpretation of the Messinian salinity crisis: controversy resolved? *Geology* **24**, 363–366 (1996).
66. Krijgsman, W. *et al.* Revised astrochronology for the Ain el Beida section (Atlantic Morocco): No glacio-eustatic control for the onset of the Messinian Salinity Crisis. *Stratigraphy* **1**, 87–101 (2004).
67. Topper, R. P. M., Flecker, R., Meijer, P. T. & Wortel, M. J. R. A box model of the Late Miocene Mediterranean Sea: Implications from combined $^{87}Sr/^{86}Sr$ and salinity data. *Paleoceanography* **26**, PA3223 (2011).
68. Krijgsman, W., Fortuin, A. R., Hilgen, F. J. & Sierro, F. J. Astrochronology for the Messinian Sorbas basin (SE Spain) and orbital (precessional) forcing for evaporite cyclicity. *Sediment. Geol.* **140**, 43–60 (2001).
69. Westerhold, T. *et al.* An astronomically dated record of Earth's climate and its predictability over the last 66 million years. *Science* **369**, 1383–1388 (2020).
70. Drury, A. J. *et al.* Late Miocene climate and time scale reconciliation: Accurate orbital calibration from a deep-sea perspective. *Earth Planet. Sci. Lett.* **475**, 254–266 (2017).
71. Herbert, T. D. *et al.* Late Miocene global cooling and the rise of modern ecosystems. *Nat. Geosci.* **9**, 843–847 (2016).
72. Laskar, J. *et al.* A long-term numerical solution for the insolation quantities of the Earth. *Astron. Astrophys.* **428**, 261–285 (2004).
73. Hilgen, F. J., Lourens, L. J. & Van Dam, J. A. The Neogene Period. in *The Geological Time Scale 2012* (eds. Gradstein, F. M., Ogg, J. G., Schmitz, M. D. & Ogg, G. M.) 947–1002 (Elsevier B.V., 2012).
74. Rohling, E. J., Schiebel, R. & Siddall, M. Controls on Messinian Lower Evaporite cycles in the Mediterranean. *Earth Planet. Sci. Lett.* **275**, 165–171 (2008).
75. Garcia-Castellanos, D. & Villaseñor, A. Messinian salinity crisis regulated by competing tectonics and erosion at the Gibraltar arc. *Nature* **480**, 359–363 (2011).
76. Krijgsman, W. & Meijer, P. T. Depositional environments of the Mediterranean "Lower Evaporites" of the Messinian salinity crisis: constraints from quantitative analyses. *Mar. Geol.* **253**, 73–81 (2008).
77. Manzi, V. *et al.* The onset of the Messinian salinity crisis in the deep Eastern Mediterranean basin. *Terra Nova* **30**, 189–198 (2018).
78. Meilijson, A. *et al.* Chronology with a pinch of salt: integrated stratigraphy of Messinian evaporites in the deep Eastern Mediterranean reveals long-lasting halite deposition during Atlantic connectivity. *Earth Sci. Rev.* **194**, 374–398 (2019).
79. Meijer, P. Th. A box model of the blocked-outflow scenario for the Messinian Salinity Crisis. *Earth Planet. Sci. Lett.* **248**, 486–494 (2006).
80. Sanford, W. E. & Wood, W. W. Brine evolution and mineral deposition in hydrologically open evaporite basins. *Am. J. Sci.* **291**, 687–710 (1991).
81. Manzi, V., Lugli, S., Roveri, M. & Schreiber, B. C. A new facies model for the Upper Gypsum of Sicily (Italy): chronological and palaeoenvironmental constraints for the Messinian salinity crisis in the Mediterranean. *Sedimentology* **56**, 1937–1960 (2009).
82. Andreetto, F. *et al.* Multi-proxy investigation of the post-evaporitic succession of the Piedmont Basin (Pollenzo section, NW Italy): a new piece in the Stage 3 puzzle of the Messinian Salinity Crisis. *Palaeogeogr. Palaeoclimatol. Palaeoecol.* **594**, 110961 (2022).
83. Rohling, E. J. *et al.* Sea level and deep-sea temperature reconstructions suggest quasi-stable states and critical transitions over the past 40 million years. *Sci. Adv.* **7**, eabf5326 (2021).
84. Rohling, E. J. *et al.* Comparison and synthesis of sea-level and deep-sea temperature variations over the past 40 million years. *Rev. Geophys.* **60**, e2002RG000775 (2022).
85. Lisiecki, L. E. & Raymo, M. E. A Pliocene-Pleistocene stack of 57 globally distributed benthic $\delta^{18}O$ records. *Paleoceanography* **20**, 1–17 (2005).
86. Dumitru, O. A. *et al.* Constraints on global mean sea level during Pliocene warmth. *Nature* **574**, 233–236 (2019).
87. Dumitru, O. A. *et al.* Sea-level stands from the Western Mediterranean over the past 6.5 million years. *Sci. Rep.* **11**, 261 (2021).
88. Hollyday, A. *et al.* A revised estimate of Early Pliocene global mean sea level using geodynamic models of the Patagonian slab window. *Geochem. Geophys. Geosyst.* **24**, e2022GC010648 (2023).
89. Bryden, H. L., Candela, J. & Kinder, T. H. Exchange through the Strait of Gibraltar. *Prog. Oceanogr.* **33**, 201–248 (1994).
90. Capella, W. *et al.* Palaeogeographic evolution of the late Miocene Rifian Corridor (Morocco): reconstructions from surface and subsurface data. *Earth Sci. Rev.* **180**, 37–59 (2018).

91. Booth-Rea, G., Ranero, C. R. & Grevemeyer, I. The Alboran volcanic-arc modulated the Messinian faunal exchange and salinity crisis. *Sci. Rep.* **8**, 13015 (2018).
92. De la Vara, A., Topper, R. P. M., Meijer, P. T. & Kouwenhoven, T. J. Water exchange through the Betic and Rifian corridors prior to the Messinian Salinity Crisis: a model study. *Paleoceanography* **30**, 548–557 (2015).
93. Bulian, F. *et al.* Impact of the Mediterranean-Atlantic connectivity and the late Miocene carbon shift on deep-sea communities in the Western Alboran Basin. *Palaeogeogr. Palaeoclimatol. Palaeoecol.* **589**, 110841 (2022).
94. Kouwenhoven, T. J., Hilgen, F. J. & Van Der Zwaan, G. J. Late Tortonian-early Messinian stepwise disruption of the Mediterranean-Atlantic connections: constraints from benthic foraminiferal and geochemical data. *Palaeogeogr. Palaeoclimatol. Palaeoecol.* **198**, 303–319 (2003).
95. Capella, W., Spakman, W., van Hinsbergen, D. J. J., Chertova, M. V. & Krijgsman, W. Mantle resistance against Gibraltar slab dragging as a key cause of the Messinian Salinity Crisis. *Terra Nova* **32**, 141–150 (2020).
96. Spakman, W., Chertova, M. V., Van Den Berg, A. & Van Hinsbergen, D. J. J. Puzzling features of western Mediterranean tectonics explained by slab dragging. *Nat. Geosci.* **11**, 211–216 (2018).
97. Jolivet, L., Augier, R., Robin, C., Suc, J.-P. & Rouchy, J. M. Lithospheric-scale geodynamic context of the Messinian salinity crisis. *Sediment. Geol.* **188–189**, 9–33 (2006).
98. Mancilla, F. L. *et al.* Slab rupture and delamination under the Betics and Rif constrained from receiver functions. *Tectonophysics* **663**, 225–237 (2015).
99. Wortel, M. J. R. & Spakman, W. Subduction and slab detachment in the Mediterranean-Carpathian region. *Science* **290**, 1910–1917 (2000).
100. Capella, W. *et al.* Thick-skinned tectonics closing the Rifian Corridor. *Tectonophysics* **710–711**, 249–265 (2017).
101. Sabino, M. *et al.* Climatic and hydrologic variability in the northern Mediterranean across the onset of the Messinian salinity crisis. *Palaeogeogr. Palaeoclimatol. Palaeoecol.* **545**, 109632 (2020).
102. Modestou, S. *et al.* Precessional variability of $^{87}Sr/^{86}Sr$ in the late Miocene Sorbas Basin: an interdisciplinary study of drivers of interbasin exchange. *Paleoceanography* **32**, 531–552 (2017).
103. Blanc, P.-L. Of sills and straits: a quantitative assessment of the Messinian Salinity Crisis. *Deep Sea Res.1* **47**, 1429–1460 (2000).
104. Amarathunga, U. *et al.* Sill-controlled salinity contrasts followed post-Messinian flooding of the Mediterranean. *Nat. Geosci.* **15**, 720–725 (2022).
105. Meijer, P. & Krijgsman, W. A quantitative analysis of the desiccation and re-filling of the Mediterranean during the Messinian Salinity Crisis. *Earth Planet. Sci. Lett.* **240**, 510–520 (2005).
106. Pellen, R. *et al.* Structural and sedimentary origin of the Gargano-Pelagosa gateway and impact on sedimentary evolution during the Messinian Salinity Crisis. *Earth Sci. Rev.* **232**, 104114 (2022).
107. Gülyüz, E., Durak, H., Özkaptan, M. & Krijgsman, W. Paleomagnetic constraints on the early Miocene closure of the southern Neo-Tethys (Van region; East Anatolia): inferences for the timing of Eurasia-Arabia collision. *Glob. Planet. Change* **185**, 103089 (2020).
108. Harzhauser, M., Piller, W. E. & Steininger, F. F. Circum-Mediterranean Oligo–Miocene biogeographic evolution – the gastropods' point of view. *Palaeogeogr. Palaeoclimatol. Palaeoecol.* **183**, 103–133 (2002).
109. Oguz, T., Özsoy, E., Latif, M. A., Sur, H. I. & Ünlüata, Ü. Modeling of hydraulically controlled exchange flow in the Bosphorus Strait. *J. Phys. Oceanogr.* **20**, 945–965 (1990).
110. Radionova, E. P. & Golovina, L. Upper Maeotian-Lower Pontian 'Transitional Strata' in the Taman Peninsula: stratigraphic position and paleogeographic interpretation. *Geol. Carpath.* **62**, 77–90 (2011).
111. Grothe, A., Sangiorgi, F., Brinkhuis, H., Stoica, M. & Krijgsman, W. Migration of the dinoflagellate *Galeacysta etrusca* and its implications for the Messinian Salinity Crisis. *Newsl. Stratigr.* **51**, 73–91 (2018).
112. Van Baak, C. G. C., Stoica, M., Grothe, A., Aliyeva, E. & Krijgsman, W. Mediterranean-Paratethys connectivity during the Messinian salinity crisis: the Pontian of Azerbaijan. *Glob. Planet. Change* **141**, 63–81 (2016).
113. Van Baak, C. G. C. *et al.* Paratethys response to the Messinian salinity crisis. *Earth Sci. Rev.* **172**, 193–223 (2017).
114. Krijgsman, W. *et al.* Mediterranean-Black Sea gateway exchange: scientific drilling workshop on the BlackGate project. *Sci. Dril.* **31**, 93–110 (2022).
115. Wegwerth, A. *et al.* Meltwater events and the Mediterranean reconnection at the Saalian–Eemian transition in the Black Sea. *Earth Planet. Sci. Lett.* **404**, 124–135 (2014).
116. Bista, D. *et al.* Sr isotope-salinity modelling constraints on Quaternary Black Sea connectivity. *Quat. Sci. Rev.* **273**, 107254 (2021).
117. Ohneiser, C. *et al.* Antarctic glacio-eustatic contributions to late Miocene Mediterranean desiccation and reflooding. *Nat. Commun.* **6**, 8765 (2015).

118. Garcia-Castellanos, D. *et al.* Catastrophic flood of the Mediterranean after the Messinian salinity crisis. *Nature* **462**, 778–781 (2009).
119. van der Laan, E. *et al.* Astronomical forcing of Northwest African climate and glacial history during the late Messinian (6.5-5.5Ma). *Palaeogeogr. Palaeoclimatol. Palaeoecol.* **313–314**, 107–126 (2012).
120. Holbourn, A. E. *et al.* Late Miocene climate cooling and intensification of southeast Asian winter monsoon. *Nat. Commun.* **9**, (2018).
121. Kontakiotis, G. *et al.* Decoding sea surface and paleoclimate conditions in the eastern Mediterranean over the Tortonian-Messinian Transition. *Palaeogeogr. Palaeoclimatol. Palaeoecol.* **534**, 109312 (2019).
122. Bulian, F., Sierro, F. J., Ledesma, S., Jiménez-Espejo, F. J. & Bassetti, M.-A. Messinian West Alboran Sea record in the proximity of Gibraltar: early signs of Atlantic-Mediterranean gateway restriction. *Mar. Geol.* **434**, 106430 (2021).
123. Fauquette, S. *et al.* How much did climate force the Messinian salinity crisis? quantified climatic conditions from pollen records in the Mediterranean region. *Palaeogeogr. Palaeoclimatol. Palaeoecol.* **238**, 281–301 (2006).
124. Vasiliev, I. *et al.* How dry was the Mediterranean during the Messinian salinity crisis? *Palaeogeogr. Palaeoclimatol. Palaeoecol.* **471**, 120–133 (2017).
125. Butiseacă, G. A. *et al.* Multiple crises preceded the Mediterranean Salinity Crisis: aridification and vegetation changes revealed by biomarkers and stable isotopes. *Glob. Planet. Change* **217**, 103951 (2022).
126. Karakitsios, V. *et al.* Messinian salinity crisis record under strong freshwater input in marginal , intermediate , and deep environments : the case of the North Aegean. *Palaeogeogr. Palaeoclimatol. Palaeoecol.* **485**, 316–335 (2017).
127. Kontakiotis, G. *et al.* Hypersalinity accompanies tectonic restriction in the eastern Mediterranean prior to the Messinian Salinity Crisis. *Palaeogeogr. Palaeoclimatol. Palaeoecol.* **592**, (2022).
128. Bertini, A. The Northern Apennines palynological record as a contribute for the reconstruction of the Messinian palaeoenvironments. *Sediment. Geol.* **188–189**, 235–258 (2006).
129. Hilgen, F. J. Astronomical calibration of Gauss to Matuyama sapropels in the Mediterranean and implication for the Geomagnetic Polarity Time Scale. *Earth Planet. Sci. Lett.* **104**, 226–244 (1991).
130. Sabino, M. *et al.* Climatic and hydrologic variability in the northern Mediterranean across the onset of the Messinian salinity crisis. *Palaeogeogr. Palaeoclimatol. Palaeoecol.* **545**, 109632 (2020).
131. Natalicchio, M. *et al.* Paleoenvironmental change in a precession-paced succession across the onset of the Messinian salinity crisis: insight from element geochemistry and molecular fossils. *Palaeogeogr. Palaeoclimatol. Palaeoecol.* **518**, 45–61 (2019).
132. Urgeles, R. *et al.* New constraints on the Messinian sealevel drawdown from 3D seismic data of the Ebro Margin, western Mediterranean. *Basin Res.* **23**, 123–145 (2011).
133. Madof, A. S., Bertoni, C. & Lofi, J. Discovery of vast fluvial deposits provides evidence for drawdown during the late Miocene Messinian salinity crisis. *Geology* **47**, 171–174 (2019).
134. Marzocchi, A. *et al.* Orbital control on late Miocene climate and the North African monsoon: insight from an ensemble of sub-precessional simulations. *Clim. Past* **11**, 1271–1295 (2015).
135. Simon, D. *et al.* Quantifying the Mediterranean freshwater budget throughout the late Miocene: New implications for sapropel formation and the Messinian Salinity Crisis. *Earth Planet. Sci. Lett.* **472**, 25–37 (2017).
136. Krijgsman, W., Stoica, M., Vasiliev, I. & Popov, V. V. Rise and fall of the Paratethys Sea during the Messinian Salinity Crisis. *Earth Planet. Sci. Lett.* **290**, 183–191 (2010).
137. Palcu, D. V. *et al.* Late Miocene megalake regressions in Eurasia. *Sci. Rep.* **11**, 1–12 (2021).
138. Sprovieri, M., Sacchi, M. & Rohling, E. J. Climatically influenced interactions between the Mediterranean and the Paratethys during the Tortonian. *Paleoceanography* **18**, 1034 (2003).
139. Gladstone, R., Flecker, R., Valdes, P., Lunt, D. & Markwick, P. The Mediterranean hydrologic budget from a Late Miocene global climate simulation. *Palaeogeogr. Palaeoclimatol. Palaeoecol.* **251**, 254–267 (2007).
140. Larrasoaña, J. C., Roberts, A. P. & Rohling, E. J. Dynamics of Green Sahara Periods and their role in hominin evolution. *PLoS One* **8**, e76514 (2013).
141. Grant, K. M. *et al.* Organic carbon burial in Mediterranean sapropels intensified during Green Sahara Periods since 3.2 Myr ago. *Commun. Earth Environ.* **3**, (2022).
142. Colin, C. *et al.* Reconstruction of Northern African monsoon between 6.2 and 4.9 Ma and possible relationships with Late Miocene events. *C. R. Geosci.* **340**, 749–760 (2008).
143. Colin, C. *et al.* Late Miocene to early Pliocene climate variability off NW Africa (ODP Site 659). *Palaeogeogr. Palaeoclimatol. Palaeoecol.* **401**, 81–95 (2014).

144. Amies, J. D., Rohling, E. J., Grant, K. M., Rodríguez-Sanz, L. & Marino, G. Quantification of African monsoon runoff during last interglacial sapropel S5. *Paleoceanogr. Paleoclimatol.* **34**, 1487–1516 (2019).
145. Bosmans, J. H. C. *et al.* Precession and obliquity forcing of the freshwater budget over the Mediterranean. *Quat. Sci. Rev.* **123**, 16–30 (2015).
146. Griffin, D. L. The late Neogene Sahabi rivers of the Sahara and their climatic and environmental implications for the Chad Basin. *J. Geol. Soc. Lond.* **163**, 905–921 (2006).
147. Griffin, D. L. Aridity and humidity: two aspects of the late Miocene climate of North Africa and the Mediterranean. *Palaeogeogr. Palaeoclimatol. Palaeoecol.* **182**, 65–91 (2002).
148. Drake, N. A. *et al.* Reconstructing palaeoclimate and hydrological fluctuations in the Fezzan Basin (southern Libya) since 130 ka: a catchment-based approach. *Quat. Sci. Rev.* **200**, 376–394 (2018).
149. Rohling, E. J. *et al.* African monsoon variability during the previous interglacial maximum. *Earth Planet. Sci. Lett.* **202**, 61–75 (2002).
150. Coulthard, T. J., Ramirez, J. A., Barton, N., Rogerson, M. & Brücher, T. Were rivers flowing across the Sahara during the last interglacial? implications for human migration through Africa. *PLoS One* **8**, e74834 (2013).
151. Wallmann, K. *et al.* Salty brines on the Mediterranean sea floor. *Nature* **387**, 31–32 (1997).
152. La Cono, V. *et al.* The discovery of Lake Hephaestus, the youngest athalassohaline deep-sea formation on Earth. *Sci. Rep.* **9**, 1679 (2019).
153. Yakimov, M. M. *et al.* Microbial community of the deep-sea brine Lake Kryos seawater-brine interface is active below the chaotropicity limit of life as revealed by recovery of mRNA. *Environ. Microbiol.* **17**, 364–382 (2015).
154. Warren, J. K. Evaporites through time: tectonic, climatic and eustatic controls in marine and nonmarine deposits. *Earth Sci. Rev.* **98**, 217–268 (2010).
155. Shields, G. A. & Mills, B. J. W. Evaporite weathering and deposition as a long-term climate forcing mechanism. *Geology* **49**, 299–303 (2021).
156. Berner, R. A. A model for atmospheric CO_2 over Phanerozoic time. *Am. J. Sci.* **291**, 339–376 (1991).
157. Lenton, T. M., Daines, S. J. & Mills, B. J. W. COPSE reloaded: an improved model of biogeochemical cycling over Phanerozoic time. *Earth Sci. Rev.* **178**, 1–28 (2018).
158. Hay, W. W. *et al.* Evaporites and the salinity of the ocean during the Phanerozoic: implications for climate, ocean circulation and life. *Palaeogeogr. Palaeoclimatol. Palaeoecol.* **240**, 3–46 (2006).
159. Nichols, G., Williams, E. & Paola, C. *Sedimentary Processes, Environments and Basins*. (Blackwell Publishing Ltd., 2007).
160. Hamilton, J. & Ford, D. Karst geomorphology and hydrogeology of the Bear Rock Formation - a remarkable dolostone and gypsum megabreccia in the continuous permafrost zone of northwest territories, Canada. *Carbonates Evaporites* **17**, 114–115 (2002).
161. Turchyn, A. V. & De Paolo, D. J. *Seawater chemistry through Phanerozoic time*. *Ann. Rev. Earth Planet. Sci.* **47**, 197-224 (2019).
162. Ivanovic, R. F., Valdes, P. J., Gregoire, L., Flecker, R. & Gutjahr, M. Sensitivity of modern climate to the presence, strength and salinity of Mediterranean-Atlantic exchange in a global general circulation model. *Clim.. Dyn.* **42**, 859–877 (2014).
163. Legg, S. *et al.* Improving oceanic overflow representation in climate models: the Gravity Current Entrainment Climate Process Team. *Bull. Am. Meteorol. Soc.* **90**, 657–670 (2009).
164. Hernández-Molina, F. J. *et al.* Onset of Mediterranean outflow into the North Atlantic. *Science* **344**, 1244–1250 (2014).
165. Bigg, G. R., Jickells, T. D., Liss, P. S. & Osborn, T. J. The role of the oceans in climate. *Int. J. Climatol.* **23**, 1127–1159 (2003).
166. Capella, W. *et al.* Mediterranean isolation preconditioning the Earth System for late Miocene climate cooling. *Sci. Rep.* **9**, 3795 (2019).
167. Adcroft, A. *et al.* The GFDL Global Ocean and Sea Ice Model OM4.0: model description and simulation features. *J. Adv. Model Earth Syst.* **11**, 3167–3211 (2019).
168. Bruciaferri, D., Shapiro, G. I. & Wobus, F. A multi-envelope vertical coordinate system for numerical ocean modelling. *Ocean Dyn.* **68**, 1239–1258 (2018).
169. Flecker, R. *et al.* https://iodp.tamu.edu/scienceops/expeditions/mediterranean_atlantic_gateway_exchange.html. (2022).
170. Bryden, H. L. & Kinder, T. H. Steady two-layer exchange through the Strait of Gibraltar. *Deep-Sea Res.* **38 (Suppl. 1)**, S445–S463 (1991).